

A deep learning framework for marine acoustic and seismic monitoring with distributed acoustic sensing

Chun Zhang^{*1,2}, Weiqiang Zhu^{1,2}, Barbara A. Romanowicz^{1,2}, Richard M Allen^{1,2}, Kenichi Soga³, and Yuxin Wu⁴

¹Department of Earth & Planetary Science, University of California, Berkeley

²Berkeley Seismology Laboratory, University of California, Berkeley

³Department of Civil & Environmental Engineering, University of California, Berkeley

⁴Earth and Environmental Sciences Area, Lawrence Berkeley National Laboratory

Abstract

Distributed Acoustic Sensing (DAS) enables high-resolution and long-duration monitoring of marine acoustic and seismic activity by turning existing fiber-optic cables into dense sensor arrays. However, extracting diverse signals from continuous DAS data remains challenging due to the massive data volumes and signal complexity. Here, we present DASNet, a deep learning framework for automated detection, classification, and arrival-time picking of diverse marine signals in DAS data. The model is trained using a semi-supervised pipeline on continuous recordings and jointly predicts spatiotemporal bounding boxes and segmentation masks for each detected event. Applied to three years of data from the Seafloor Fiber-Optic Array in Monterey Bay (SeaFOAM), DASNet identified over 500,000 events spanning multiple signal categories. For seismic monitoring, the model detects the majority of cataloged local earthquakes within 100 km and identifies distant earthquake-generated T-waves, with beamforming analysis revealing source azimuths clustered toward the southwestern Pacific and along mid-ocean ridge systems. For bioacoustic monitoring, DASNet detects and tracks more than 400,000 blue and fin whale calls, revealing seasonal and interannual variability consistent with independent hydrophone records. For anthropogenic activity, DASNet detects and localizes vessel traffic near the cable, with estimated positions validated against Automatic Identification System (AIS) tracks. These results demonstrate that combining DAS with deep learning provides a scalable, high-resolution monitoring approach for marine environmental observation. As submarine DAS deployments expand, this framework could substantially enhance seismic, bioacoustic, and anthropogenic observations in regions where conventional instrumentation remains sparse.

1 Introduction

The open ocean carries acoustic and seismic signals from tectonic, biological, and anthropogenic sources that interact across spatial scales from regional to basin-wide and over timescales from seconds to decades. Natural hazards such as earthquakes, submarine landslides, and volcanic eruptions reshape the seafloor and, in some cases, generate tsunamis that affect distant coastlines (e.g., Carvajal et al., 2022; Harbitz et al., 2006; Kanamori, 1972; Omira et al., 2022), with cascading effects on benthic habitats and industrial infrastructure (e.g., Thomsen et al., 2021; Seike et al., 2013). Biological and anthropogenic activities jointly modulate the marine acoustic environment. Whales and other megafauna communicate using low-frequency acoustics, while expanding shipping traffic, offshore wind farms, and seabed infrastructure impose persistent acoustic and mechanical stress on ocean ecosystems (e.g., Roman et al., 2014; Ryan et al., 2022; Erbe et al., 2019; Hildebrand, 2009; Ryan et al., 2025). Despite the scientific and societal importance of these phenomena, routine offshore observations remain sparse and episodic. Conventional ocean-bottom seismometers and

*Correspondence to: chun.zhang@berkeley.edu

hydrophones are costly to deploy, limited in spatial and temporal coverage, and typically restricted to short-term campaigns (Toomey et al., 2014; Suetsugu & Shiobara, 2014), leaving hazards under-detected, biodiversity trends under-sampled, and anthropogenic impacts insufficiently quantified.

Distributed Acoustic Sensing (DAS) offers a promising direction to address this observational gap by converting existing submarine fiber-optic cables into dense sensor arrays. DAS measures minute strain or strain-rate changes in optical backscatter, enabling continuous, high-resolution monitoring at reduced deployment costs (Zhan, 2020; Lindsey et al., 2019; Lindsey & Martin, 2021; Williams et al., 2019; Romanowicz et al., 2023; Trafford et al., 2022). Over the past several years, DAS has been used to detect earthquakes, marine mammal vocalizations, and anthropogenic signals such as vessel traffic and infrastructure operations, demonstrating its potential for integrated, long-duration ocean observation (e.g., Williams et al., 2019; Sladen et al., 2019; Ide et al., 2021; Lior et al., 2021, 2022; Williams et al., 2022; Landrø et al., 2022; Bouffaut et al., 2022; Biondi et al., 2023; Z. Shen & Wu, 2024; Xiao et al., 2024; Tonegawa & Araki, 2024; Gou et al., 2025; Xenaki et al., 2025). However, realizing the full potential of DAS poses substantial challenges. Data quality varies with cable design, installation conditions, and coupling to the surrounding medium (Wang et al., 2018; Lindsey et al., 2020; Paitz et al., 2021; Muir & Zhan, 2022), so portions of a DAS recording may be dominated by noise or exhibit low sensitivity to certain sources. In addition, DAS records often contain superposed wavefields that mix seismic phases, ocean acoustic signals, anthropogenic noise, and other environmental signatures across frequency bands spanning millihertz to hundreds of hertz, each with distinct apparent velocities and coherence lengths, complicating the isolation and attribution of individual sources. At the same time, DAS acquisitions generate terabytes of data per day from thousands of channels, making manual inspection impractical for event detection and characterization (Ma et al., 2023; Romanowicz et al., 2023). These factors motivate the development of automated and scalable analysis methods for DAS.

Recent advances in machine learning provide powerful tools for addressing challenges in automated and scalable DAS data analysis. Neural networks can learn representations directly from raw waveforms, enabling efficient and accurate detection across diverse signal types. In seismology, machine learning has improved seismic phase picking (e.g., Zhu & Beroza, 2019; Mousavi et al., 2020; Sun et al., 2023), phase association (e.g., Ross et al., 2019; Zhang et al., 2019; Zhu, McBrearty, et al., 2022; Zhu, Tai, et al., 2022), and waveform denoising (e.g., Zhu et al., 2019; S. Yu et al., 2019). However, these advances have largely relied on decades of accumulated high-quality labeled data from traditional seismic networks. No comparable training corpus exists for DAS, despite the rapid expansion of DAS deployments. Moreover, DAS recordings exhibit characteristics that differ from conventional seismograms, including strong directional sensitivity, variable cable coupling, coherent noise patterns, frequent superposition of multiple sources, and non-standard data formats (Wang et al., 2018; Lindsey et al., 2019; Paitz et al., 2021; Muir & Zhan, 2022; Näsholm et al., 2022; Adeniyi et al., 2025). These factors necessitate specialized approaches that extend beyond simple adaptation of existing seismic models. Supervised DAS models trained on carefully annotated subsets have demonstrated the ability to detect microseismic and other weak signals that conventional methods often miss, but their applicability remains constrained by labeling cost and generalization across arrays (Huot et al., 2022; Lv et al., 2023; Ma et al., 2023; P. Yu et al., 2024; Boitz & Shapiro, 2024; Xiao et al., 2026). Unsupervised and self-supervised approaches provide a complementary strategy by learning stable representations from continuous DAS streams without manual labels, though they typically require a downstream task or a small labeled set to transfer learned features into usable detections (Zhu et al., 2023; Van den Ende et al., 2021; Ding et al., 2025; J. Shen & Zhu, 2026). Despite these advances, few existing methods generalize across multiple DAS signal types simultaneously. This limitation reflects both the complexity of DAS wavefields and the specialized training each signal class demand. This represents a critical gap for submarine DAS applications, which record diverse physical phenomena spanning seismic, bioacoustic, and anthropogenic sources. A unified detection framework would enable integrated analysis across these signals, offering opportunities across geophysics, oceanography, and environmental monitoring.

Here we present DASNet, a deep learning framework for automated detection, classification, and arrival-time picking of diverse marine signals in DAS data. DASNet processes multi-frequency input channels and jointly predicts spatiotemporal bounding boxes and segmentation masks, representing each detected event as a structured object for downstream analysis. The model is trained using a semi-supervised pipeline that iteratively improves on continuous recordings, making it practical for long DAS deployments where labeled data are limited but unlabeled data are abundant. We apply DASNet to over three years of SeaFOAM data from Monterey Bay (Romanowicz et al., 2023) and show that a unified model can support four rep-

representative marine monitoring tasks: (i) detecting local earthquakes and measuring phase arrival times for source localization; (ii) identifying T-waves generated by distant earthquakes and estimating source azimuths via beamforming; (iii) cataloging baleen whale calls to reveal seasonal and interannual behavioral patterns; and (iv) monitoring of anthropogenic signals such as tracking vessel traffic near the cable. These examples demonstrate that DASNet can transform continuous fiber-optic recordings into structured multi-class event catalogs without task-specific preprocessing. As submarine fiber-optic networks continue to expand worldwide, coupling DAS with scalable machine learning could fundamentally enhance our capacity to observe seismicity, marine ecosystems, and human activity across ocean basins that remain beyond the reach of traditional instrumentation.

2 Methods

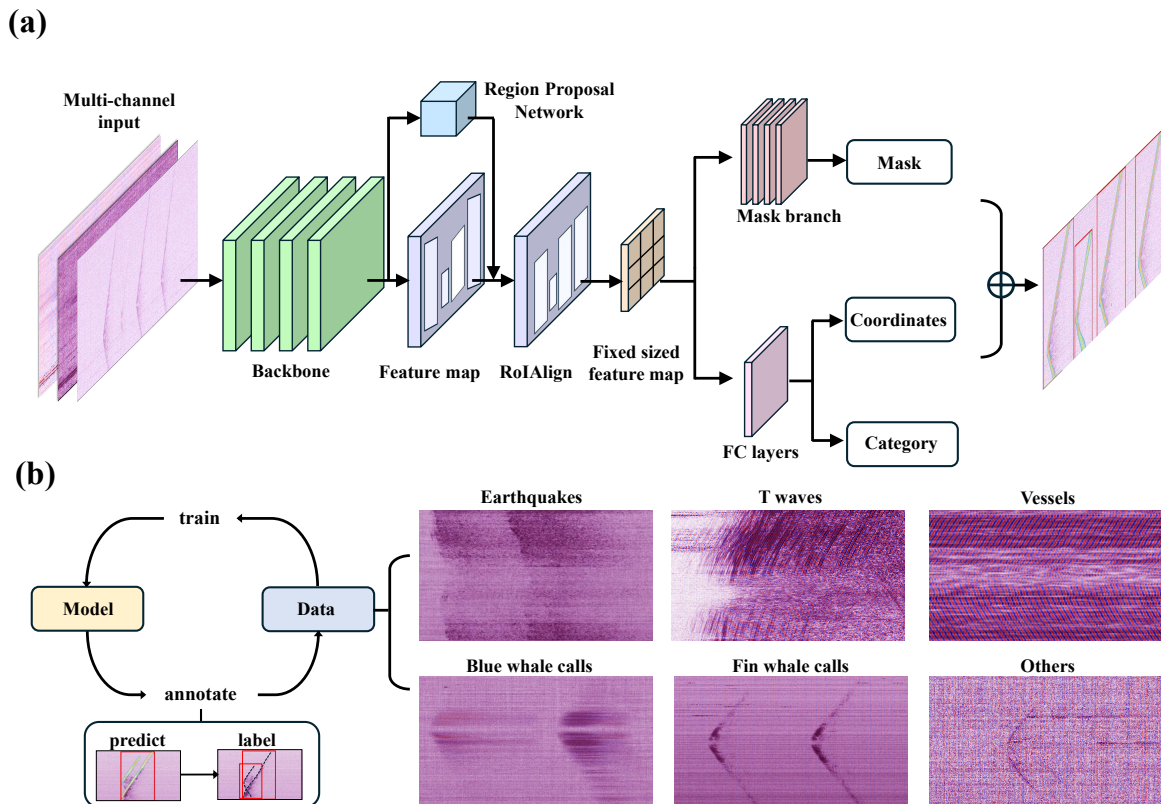


Figure 1: DASNet framework overview. (a) Model architecture with the feature extraction backbone, region proposal network, and output branches for classification, bounding box regression, and mask prediction. (b) Semi-supervised data engine workflow for iterative dataset expansion and model refinement. Only a subset of whale call categories is shown here; the complete set is presented in Figure 3.

2.1 Neural network architecture

DASNet (Figure 1a) adapts Mask R-CNN, a deep learning framework designed for simultaneous object detection and instance segmentation (He et al., 2017), to detect and measure diverse seismic and acoustic signals in DAS recordings. For each detected instance, the model produces three outputs: (1) a bounding box delineating the spatial-temporal extent of the signal, (2) a classification label with an associated confidence score, and (3) a probability mask over channels and time that highlights arrival energy and supports arrival-time estimation. By treating each event as a discrete object in the 2D channel-time domain, this approach

departs from conventional channel-wise detectors and naturally handles monitoring conditions where multiple sources overlap in time and across channels.

The DASNet architecture consists of four primary components: a feature extraction backbone, a Region Proposal Network (RPN), a Region of Interest Align (ROIAlign) module, and multiple output branches for classification, bounding box regression, and mask generation. It follows the two-stage design of Mask-RCNN that yields accurate instance masks and stable localization at moderate computational cost. In the first stage, a convolutional backbone with a Feature Pyramid Network (FPN) extracts multiscale representations that capture both local waveform characteristics and array-wide patterns. We employ ResNet-50 (He et al., 2016) with FPN, which provides a good balance between accuracy and training stability for long sequences. Alternative backbones such as Vision Transformer, Swin Transformer or ConvNeXt (Dosovitskiy, 2020; Liu et al., 2021, 2022) may improve accuracy but were not explored here, as the present effort emphasizes establishing a reproducible baseline. Then, region proposals are generated by the RPN and are refined by ROIAlign to preserve alignment between features and the underlying channel-time grid. In the second stage, three prediction branches operate on each proposed region. The classification branch assigns an event type, the regression branch refines the spatiotemporal bounding box, and the mask branch predicts a high-resolution probability mask from which arrival-time trajectories are extracted.

The model architecture has been optimized to balance computational efficiency and performance, given the high-resolution nature of DAS data. We added additional downsampling in the backbone by modifying the stride and downsampling behavior of early convolutional blocks. This reduces the resolution of intermediate feature maps and substantially lowers computational cost while preserving event-scale semantic information required for detection and segmentation. The FPN was configured with a reduced channel dimension compared to the standard Mask R-CNN implementation, further improving memory efficiency. We also revised the mask prediction branch by cropping input features to address the spatiotemporal aspect ratio imbalance of DAS signals. Since DAS provides continuous data where signals can span much longer temporal durations than spatial extent, this differs substantially from conventional image-based tasks. This cropping strategy maintains a more consistent aspect ratio for the learning target of the mask head. Detailed model configurations and implementation details are provided in Text S1 of the Supplementary Information. Beyond architectural modifications, the input representation was designed to enhance feature extraction across the diverse spectral characteristics of DAS signals. We employ a multi-channel input strategy that encodes information from three frequency bands: (1) raw strain rate, which retains the full broadband signal to preserve critical features; (2) bandpass-filtered strain (2-10 Hz), which highlights low-frequency signals including local earthquakes and T-waves; (3) high-pass filtered strain (>10 Hz), which emphasizes high-frequency signals, such as whale calls and vessel noise. This structured input design enables the model to effectively learn the spectral characteristics of different signal types and enhances its ability to distinguish among geophysical, biological, and anthropogenic sources.

2.2 Semi-supervised data engine

The rapid expansion of global DAS networks has generated vast data volumes (e.g., Wuestefeld et al., 2024). However, the lack of a comprehensive annotated dataset poses a major challenge for supervised learning approaches. As fully manual annotation is impractical given the scale of DAS data, we apply a semi-supervised data engine to facilitate annotation and dataset expansion (Figure 1b). The data engine operates in two distinct stages: (1) an initial manual annotation stage, and (2) a semi-automatic stage where model-generated predictions assist human annotation.

In the first stage, a subset of DAS data is manually reviewed and labeled to establish a preliminary dataset. Each annotated instance includes three components: a bounding box capturing the full signal extent, a categorical label indicating the signal type, and a manually picked signal arrival-time curve. The mask representation is generated as a Gaussian distribution centered on the picked time curve. This probabilistic representation mitigates inconsistencies introduced by human labeling errors (Zhu & Beroza, 2019) and provides the model with a structured learning target. We split this dataset into training and test sets at an 8:2 ratio. Each input segment has an input size of $12,000 \times 2,845$ (60 s at 200 Hz sampling rate across 2,845 channels) and is filtered to produce multi-channel model input, with each segment normalized independently. To expand data diversity, we applied stochastic data augmentation: superposing synthetic noise to improve robustness to low SNR events, applying random spatial flips and slight stretching (temporal

and spatial resampling) to enhance generalization across different DAS configurations; and stacking multiple signals to sharpen the model’s ability to separate overlapping instances. The model trained on this augmented dataset then served as the starting point for the second phase. For training, we used AdamW optimizer with a weight decay of 1×10^{-4} . The initial learning rate was set to 1×10^{-4} with a cosine decay schedule and a linear warm-up over the first epoch. The models were trained for 15 epochs using an effective batch size of 6.

Once the initial model was trained, the data engine transitioned into the semi-supervised iterative phase. The model was deployed on continuous DAS recordings, generating predictions despite limited initial accuracy. The predicted bounding boxes and categorical labels were retained, and the signal arrival-time curves were extracted from the probability distribution masks. These preliminary annotations were then manually reviewed and refined before being incorporated into the dataset. The updated dataset was subsequently used to retrain the model, enhancing its detection and measurement capabilities. Throughout this process, we kept the dataset splitting ratio as 8:2 and applied the same training strategy. This iterative process progressively improved the model performance, which in turn accelerated subsequent dataset expansion in a self-reinforcing cycle. For example, the annotation efficiency increases with each iteration. Early stages require significant manual correction of low-quality model prediction, making annotation time-consuming, whereas later stages produce automatic labels of sufficient quality, requiring only minimal human intervention. Eventually, the data engine achieves a near-automatic state, enabling large-scale dataset expansion with minimal manual effort.

2.3 The SeaFOAM dataset

In this study, we conducted the entire model iteration, signal detection, and arrival-time picking workflow on the SeaFOAM (Seafloor Fiber-Optic Array in Monterey bay) dataset (Romanowicz et al., 2023). The SeaFOAM experiment utilizes DAS technology deployed on the 52 km submarine cable offshore Monterey Bay, California, with data acquisition beginning on July 21, 2022. The system records data at 200 Hz sampling rate from 10,245 channels with 5.1 m spatial resolution. The SeaFOAM DAS data capture a wide range of seismic and oceanic signals, including local and teleseismic events, ocean currents, water waves, ambient noise, and marine mammal vocalizations. Note that the water depth varies significantly along the cable, so the background noise characteristics change accordingly, with much higher noise levels in shallow water. For this reason, we focused on the deep-water section (channels 7,400-10,245, >200 m depth and ~37.6-52 km distance from shore) with better signal quality (Figure 2).

We initiated the first phase of the data engine using records from August 2022, because this period coincides with known whale activity offshore of California (e.g., Wiggins et al., 2005). We conducted a rough manual search for signals of interest, including earthquake signals and several types of whale calls. This small dataset was used to train the first model, which then served as the starting point for the second phase of iteration. In subsequent rounds, we applied the model to continuous data to expand the dataset and re-train updated models. Early iterations applied the model to shorter time spans for rapid feedback, and later iterations extended to longer archives as detection quality stabilized. At each stage, we performed time-uniform sampling to select a representative and diverse subset of predictions for manual review and model refinement. Given the substantial class imbalance among signal types, we controlled the number of samples selected per class to ensure adequate representation and applied oversampling to amplify underrepresented classes. Through successive iterations, the model’s performance improved significantly, ultimately yielding detections of over 500,000 events across the full dataset.

3 Results

3.1 Multi-class signal detection and arrival-time measurement

Automated multi-class signal detection in marine DAS data poses significant challenges because the signals of interest span a wide range of spatiotemporal scales and spectral characteristics (Figure S1). For example, local earthquake signals primarily exhibit energy below 10 Hz, while teleseismic arrivals are typically strongest below 1 Hz. Marine mammal vocalizations occupy distinct frequency bands. Fin whale calls appear around 15-25 Hz, while blue whale calls contain multiple harmonics from 10 Hz upward. Vessel-generated noise is

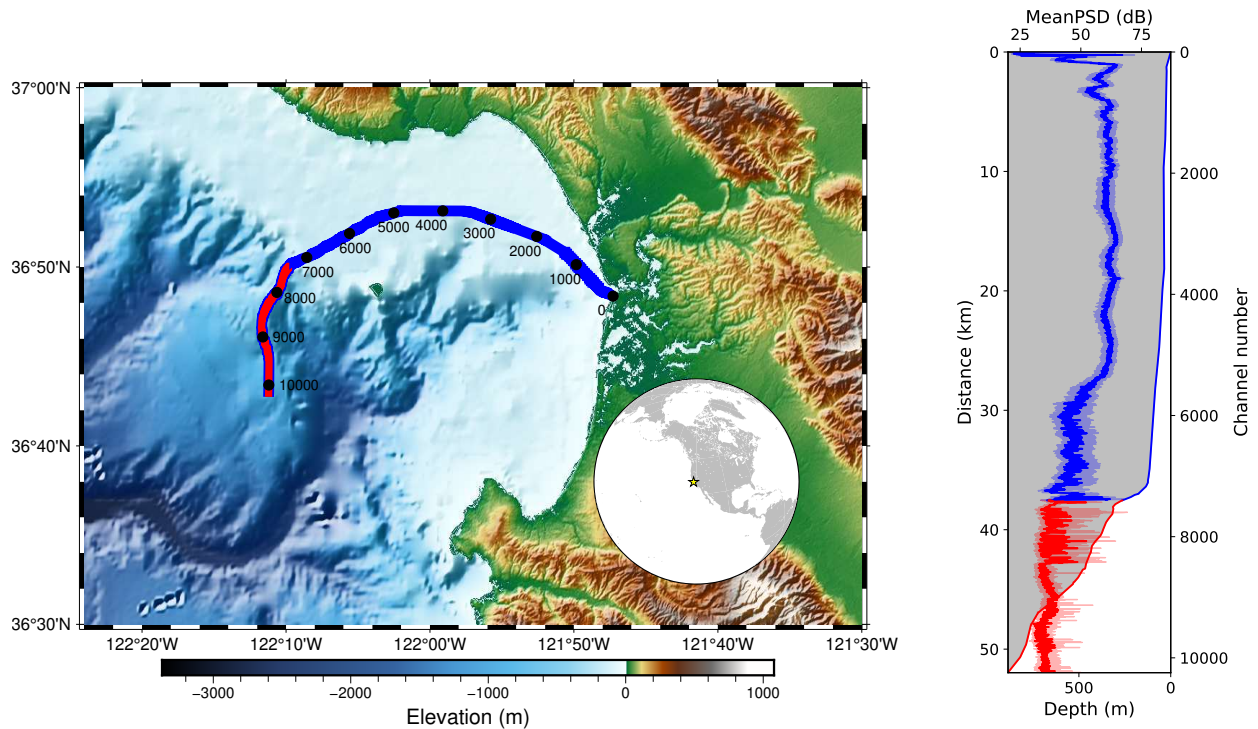


Figure 2: SeaFOAM DAS array configuration and data characteristics. (a) Location of the SeaFOAM DAS array. The red line denotes the section used in this study, whereas the blue line indicates the unused portion. Black dots mark every 1,000 channels along the cable from the interrogator unit. The inset in the lower right shows the location of the cable in Monterey Bay, California. (b) Depth profile of the underwater DAS channels, overlaid with the daily median power spectral density (PSD) for each channel on 25 November 2023 (solid line). Shaded areas represent the 10th - 90th percentiles of PSDs, illustrating channel-to-channel signal variation.

often characterized by narrowband peaks above 10 Hz. This broad spectral diversity limits both traditional signal processing methods and single-task machine learning models, which struggle to generalize across signal categories. By leveraging multi-frequency input with different frequency bands as separate channels, DASNet can effectively process complex DAS data containing diverse spectral features. Figure 3(a) shows representative examples of the signal types observed across sections of the DAS array. Though acoustic and seismic signals vary significantly in frequency content, amplitude, and temporal structure, DASNet successfully classifies, localizes (via bounding boxes), and measures arrival times for these events. The applicable categories include seismic events (P-, S-, and T-waves), marine mammal calls (blue whale A, B, and D calls; fin whale calls), anthropogenic sources (vessel noise), and short-duration signals of unknown origin.

We evaluated DASNet on a held-out test set constructed from SeaFOAM recordings, and the model reliably detected signals across all categories (Figure 3b). For signals that are typically strong and well-structured, such as earthquake signals, T-waves, and fin whale calls, DASNet achieved high accuracy with F1 scores typically >0.9 . This strong performance is largely attributable to the rich and diverse training dataset constructed through semi-supervised iterations (see Methods), which enabled the model to capture representative characteristics of each signal type. Manual inspection of failed predictions revealed that most missed detections and false positives arose from poor signal quality due to inherently weak signals or strong background noise, or from truncated waveforms at segment boundaries. For example, fin whale call detection (best F1 = 0.87) was affected by faint signals from distant sources, where seismic S-wave detections (best F1 = 0.9) benefited from the typically strong and sustained character of these arrivals. Blue whale D calls proved more difficult to detect, primarily because of their scarcity and variability, leaving them underrepresented in the training data and limiting the model’s ability to generalize.

We further evaluated the choice of detection threshold, which is a critical trade-off in operational applications, on continuous data. Higher thresholds yield fewer but higher-quality detections (Figure S2). We observed that the detection counts at lower score thresholds exhibit the same temporal variability as high-quality detections, with both increasing and decreasing coherently across time windows. Moreover, periods with few or no high-score detections do not show an emergence of additional detections at lower thresholds. This consistent temporal co-variation indicates that low-score detections are predominantly associated with the same underlying signal activity, rather than representing spurious false positives. In subsequent analyses, we adopted a relatively stringent threshold (0.8) to ensure the quality of detections.

In addition to detecting acoustic and seismic events, precise measurement of their arrival times is essential for scientific analyses such as source localization and subsurface structure imaging. We evaluated the arrival-time accuracy using manually annotated or reviewed arrival picks for signals with clear and consistent onsets, such as blue whale B calls, fin whale calls, earthquake P- and S-waves, and short-duration unknown signals. Figure 3(c) shows that DASNet achieved high timing precision for marine mammal vocalizations, with mean absolute errors of 0.15 s (standard deviation 0.20 s) for blue whale B calls; and a mean of 0.08 s (standard deviation 0.11 s) for fin whale calls. The short-duration unknown signals with sharp onsets show the highest accuracy (a mean of 0.06 s and a standard deviation of 0.10 s). Seismic phases exhibited lower timing precision, with a mean of approximately 0.17 s (standard deviation 0.24 s) for P-waves, and a mean of 0.15 s (standard deviation of 0.21 s) for S-waves. Overall, the achieved arrival-time precision is sufficient for downstream analyses such as event localization and subsurface structure imaging, across different acoustic and seismic signal types.

The experiments above demonstrate that DASNet can effectively detect and measure marine acoustic and seismic signals, expanding DAS’s utility across diverse scientific disciplines. In the subsequent sections, we apply the trained model to three years of continuous SeaFOAM recordings to explore its potential for several environmental and geophysical monitoring applications.

3.2 Local earthquake detection and localization

Seismic monitoring in offshore regions has long been limited by sparse instrumentation coverage. DAS presents a promising approach to address this data gap by providing dense spatial sampling along existing submarine cables (e.g., Williams et al., 2019; Fernández-Ruiz et al., 2022). Realizing this potential requires automated methods for phase detection and arrival-time picking that can operate reliably on continuous, high-volume DAS recordings. The earthquake detection and phase-picking capabilities of DASNet

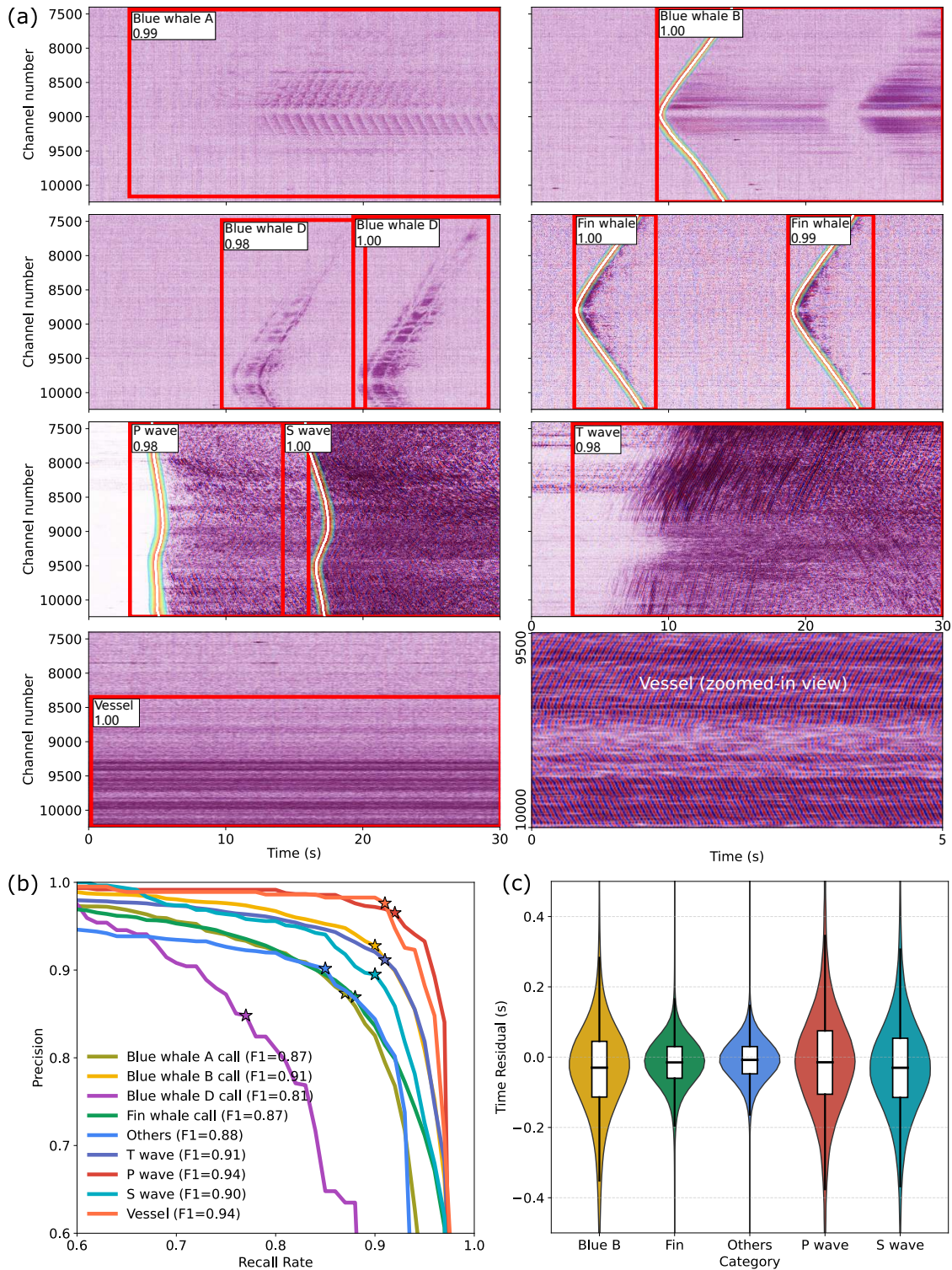


Figure 3: Model performance evaluation and signal examples. (a) Representative examples of each signal type detected in the SeaFOAM dataset. Earthquake and T-wave segments are bandpass filtered between 2–10 Hz, while the remaining signals are highpass filtered above 10 Hz to enhance relevant features. The corresponding spectrograms are shown in Figure S1. (b) Precision-recall (PR) curves for all signal categories evaluated on the test set at an intersection-over-union (IoU) threshold of 0.5. Stars on each curve mark the point corresponding to the highest F1 score. (c) Distribution of arrival-time residuals on the test set, computed as the difference between predicted and manually labeled arrival times. Predicted arrivals are extracted as the peak of the model’s probability mask using a threshold of 0.5. Boxplots display the median (bold horizontal line), interquartile range (IQR; box boundaries), and whiskers extending to $1.5 \times \text{IQR}$ from the quartiles. Outliers beyond this range are omitted for clarity.

could therefore enable DAS to improve the coverage and resolution of offshore earthquake monitoring and subsurface imaging (Gou et al., 2025; Biondi et al., 2023; Miao et al., 2025).

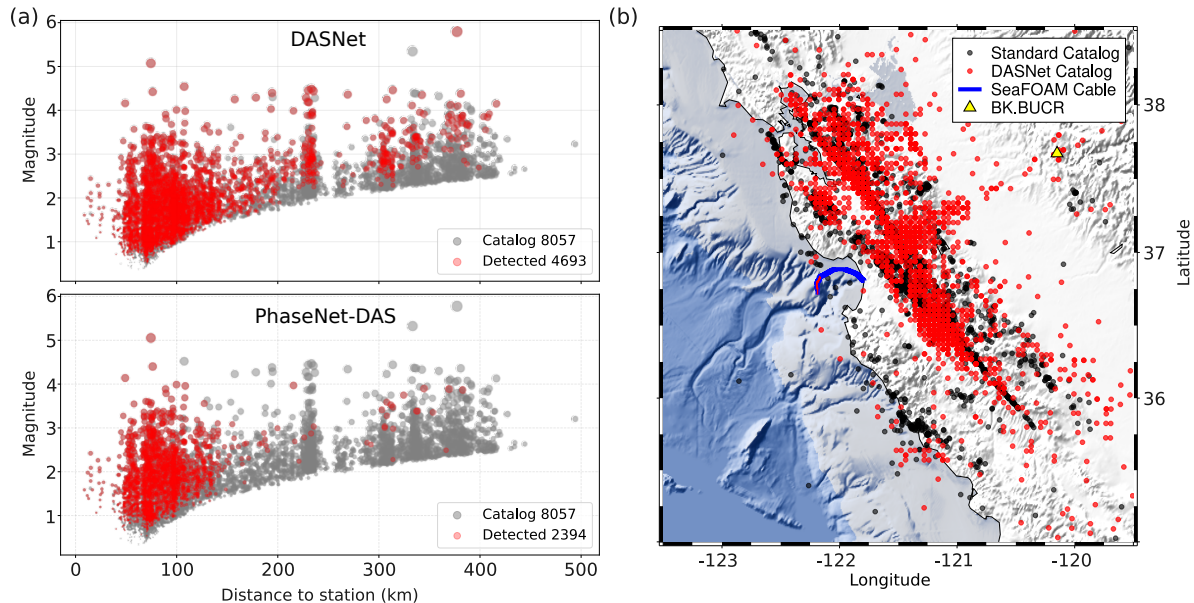


Figure 4: Earthquake detection and localization results. (a) Comparison of the earthquake detection performance between DASNet and PhaseNet-DAS as a function of event magnitude and epicentral distance, where the distance is computed relative to the average location of the DAS cable. (b) Earthquake epicenters determined by combining P- and S-phase arrival times picked by DASNet on SeaFOAM DAS and by PhaseNet on the conventional seismic station BK.BUCR.

To evaluate DASNet’s performance in detecting real earthquake signals, we selected earthquakes from the Northern California Seismic Network (NCSN) catalog that occurred between 2022 and 2025 within a region around the cable, bounded by coordinates $124^{\circ}00' W$, $117^{\circ}46' W$ and $34^{\circ}30' N$, $40^{\circ}00' N$. Due to the limited spatial coverage of the DAS cable compared to the regional seismic network, signals from distant small-magnitude earthquakes are expected to be too weak to be detected by DAS. Thus, we filtered the catalog based on an approximate magnitude-distance scaling relation (Yin et al., 2023). To establish a reference baseline, we applied the pre-trained PhaseNet-DAS model to the same time period, using a low confidence threshold (0.3) to maximize recall at the expense of increased false positive. As shown in Figure 4(a), DASNet demonstrated superior robustness in detecting small-magnitude events near the DAS array and achieved a lower detection threshold compared with PhaseNet-DAS. This enhanced performance partly arises from differences in model design. PhaseNet directly detects phase arrivals from continuous data, while DASNet first performs event detection via a bounding box, then picks precise phase arrivals within the detected window. This two-stage design facilitates DASNet in recognizing coherent signal features across longer temporal windows, enabling the detection of faint earthquake signals even when phase arrivals are difficult to identify.

Using these DASNet-derived picks, we further estimated earthquake source locations. The resulting epicenters broadly reproduce the spatial patterns of cataloged seismicity (Figure S3), validating the reliability of DASNet picks. However, some event locations remain poorly constrained, particularly for events at greater distances from the cable, due to limited azimuthal coverage inherent to a single DAS array. Combining DAS with conventional seismic stations can directly address this limitation. As an example, we integrated the DASNet picks with PhaseNet picks from a broadband seismic station (BK.BUCR). Compared with the DAS-only locations (Figure S3), the joint inversion yields more stable location estimates and improved agreement with the cataloged seismicity distribution (Figure 4b). These results highlight that future efforts combining DAS with seismic networks, leveraging multiple cables, or deploying cables with optimized geometries could significantly enhance both localization accuracy and spatial coverage for offshore earthquake monitoring.

3.3 T-wave detection and source azimuth estimation

T-waves are acoustic phases generated when seismic body waves convert into acoustic energy at the seafloor and propagate efficiently through the ocean’s sound fixing and ranging (SOFAR) channel over thousands of kilometers (Tolstoy & Ewing, 1950). Because they are commonly excited by distant offshore earthquakes or volcanic eruptions, T-waves offer a valuable window to monitor offshore and deep-ocean seismicity in regions poorly covered by conventional seismic networks (Dziak et al., 2004; Fox et al., 2001; Hanson & Bowman, 2006; Parnell-Turner et al., 2022; Smith et al., 2002; Tepp & Dziak, 2021; Wech et al., 2018). Furthermore, T-waves from stable and repeatable source-receiver paths also enable ocean thermometry through time-lapse measurements of sound-speed variations (Wu et al., 2020). However, seismic stations capable of capturing T-waves remain sparsely distributed across the ocean. DAS has proven effective for T-wave detection (Z. Shen & Wu, 2024). In addition to enabling long-term continuous monitoring, the dense spatial sampling of DAS arrays allows the constraint of source azimuth via beamforming techniques (van den Ende & Ampuero, 2021).

During the 3-year SeaFOAM observation period, DASNet detected over 68,000 T-wave events, which is far more than the number of earthquakes reported for the same interval. This highlights the sensitivity of DAS to far-field acoustic energy from global seismic sources. To investigate their origins, we estimated the back-azimuth of each detection by applying beamforming to 2-10 Hz bandpass-filtered data and retaining energy with apparent speeds near 1.5 km/s through an f-k filter. The azimuth at maximum beam power was taken as the most probable direction of arrival. The resulting azimuthal distribution in Figure 5 reveals three distinct azimuthal clusters. The first cluster is characterized by predominantly southern back azimuths, consistent with sources along the Southeast Pacific spreading system. The second cluster exhibits southwestern back azimuths, indicating energy arriving from the Tonga-Vanuatu subduction zone. The third cluster is associated with western back azimuths, suggesting potential contributions from the Izu-Bonin-Mariana (IBM) arc region. Note that these back-azimuths describe propagation directions rather than unique source epicenters. The actual sources may lie anywhere along each great-circle path. Azimuthal constraints are weaker for southern back azimuths because of the cable geometry, leading to larger uncertainties. This ambiguity can be reduced with longer or curved cable layouts (Figure S4).

To further constrain source locations and verify azimuths identified by DASNet, we applied multi-array localization using simultaneous detections from SeaFOAM and two additional DAS arrays (Figure 5 and Figure S5). We applied triangulation based on independent azimuthal estimates from separate cables to obtain constraints on remote source locations. In the first case, we used a 4-day overlapping deployment between the SeaFOAM DAS and the Ocean Observatory Initiative (OOI) Regional Cabled Array in May 2024, during which multiple coincident T-wave events were recorded (Romanowicz et al., 2023; Lipovsky, 2024; Shi et al., 2024). A representative event on May 8, 2024 (observed at 13:38:05 UTC on OOI and 13:35:54 UTC on SeaFOAM) was jointly analyzed. The intersection of the two azimuthal estimates closely aligns with the epicenter of a Mw 5.2 earthquake that occurred offshore Vanuatu at 11:51:39 UTC. The predicted T-wave travel times agree with the observed arrivals on both DAS arrays, validating the multi-array localization method and confirming the southwestern Pacific as a T-wave source region. In the second case, we localized another coincident event recorded by SeaFOAM and the offshore Chile F1 DAS network operated by the French Seismological and Geodetic Network (RESIF) (Rivet et al., 2025). On May 14, 2025, both arrays recorded a T-wave whose triangulated source location falls on the Pacific-Antarctic Ridge, coinciding with a Mw 5.2 earthquake at 16:33:05 UTC. Because the F1 DAS array data are provided at a 5-km spatial interval, the beamforming results are degraded due to spatial aliasing. These two case studies demonstrate the effectiveness of multi-array DAS localization for constraining remote seismic sources. The agreement with known earthquake epicenters reinforces DASNet’s detection reliability and showcases the potential of combining globally distributed DAS arrays. As long-duration submarine deployments continue to expand, this approach offers promising capabilities for more precisely monitoring seismic and volcanic activity across ocean basins that remain beyond the reach of traditional seismic networks.

3.4 Tracking bioacoustic and anthropogenic sources

Vocalizations are central to the life history of many marine species, particularly baleen whales, which rely on low-frequency vocalizations for communication and navigation across vast oceanic distances (e.g., R. S. Payne & McVay, 1971; R. Payne & Webb, 1971; Tyack, 2008). Fin whales (*Balaenoptera physalus*) and blue whales

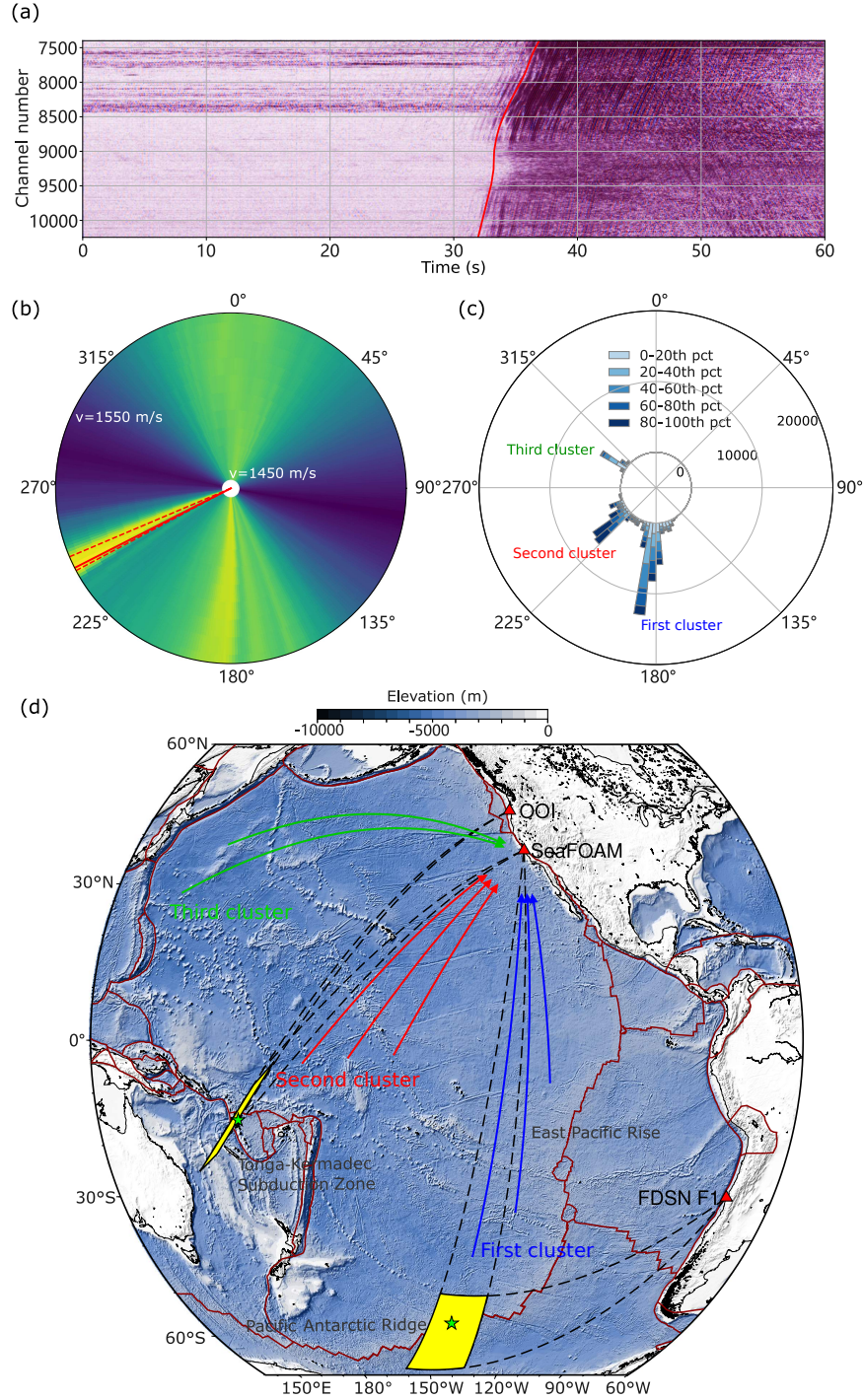


Figure 5: T-wave detection and multi-array source localization. (a) T-wave waveforms recorded by the SeaFOAM cables, beginning at 2024-05-08 13:35:22 UTC. The red line indicates the theoretical arrival times computed from the estimated T-wave azimuth shown in (b) for the Vanuatu event (assuming a propagation velocity of 1.46 km/s, which provides the best fit to the observed signal onset), showing close agreement with the observed waveforms. (b) Heat maps derived via beamforming for azimuthal estimation. (c) Distribution of estimated T-wave source azimuths. Color shading within each azimuth bin indicates the distribution of signal amplitudes, with darker colors representing stronger arrivals. Three prominent azimuthal clusters are observed. (d) Map showing the locations of the SeaFOAM, OOI, and RESIF F1 DAS installations (Romanowicz et al., 2023; Shi et al., 2024; Rivet et al., 2025). Arrows indicate the dominant azimuths of T-wave arrivals detected over the 3-year period. Yellow regions and dashed lines illustrate two examples of multi-array localization through azimuthal triangulation. Green star mark the epicenters of two earthquake events (Mw 5.2, 2024-05-08 11:51:39 UTC, Vanuatu; and Mw 5.2, 2025-05-14 16:33:05 UTC, Pacific-Antarctic Ridge) corresponding to the observed T-waves.

(*Balaenoptera musculus*) produce particularly powerful and stereotyped calls (e.g., McDonald et al., 1995; Lavery et al., 2014; Roman et al., 2014; Barlow et al., 2023; Simon et al., 2010; Ryan et al., 2022; Oestreich et al., 2022, 2020; Au & Hastings, 2008; Širović et al., 2007), making them well suited for passive acoustic monitoring (PAM). PAM has become a key tool for studying the spatial distribution and seasonal migration patterns of these species, especially in remote or visually inaccessible regions (McDonald et al., 1995; Širović et al., 2007; Au & Hastings, 2008; Richardson et al., 2013; Oestreich et al., 2024). However, conventional PAM systems, such as hydrophone arrays, are often limited by sparse deployment and low spatial resolution (Eguíluz et al., 2016; Ahonen et al., 2021, e.g.). Recent studies have shown that DAS is capable of capturing whale vocalizations even in challenging environments and can be used for identifying and tracking the whale behaviors (Bouffaut et al., 2022; Landrø et al., 2022; Wilcock et al., 2023; Xiao et al., 2025; Saw et al., 2025; Goestchel et al., 2025). DASNet’s ability to automatically detect and classify diverse whale calls at scale enables long-term monitoring of seasonal distribution and behavior patterns across multi-year DAS deployments. We further leverage the model’s capacity for vessel tracking to demonstrate a promising direction for quantifying anthropogenic noise exposure and its potential impact on marine ecosystems.

During the monitoring period, the SeaFOAM DAS array recorded extensive vocalizations from fin and blue whales, including more than 320,000 fin whale calls and over 80,000 blue whale calls. The temporal distribution of these detections reveals distinct seasonal patterns consistent with known migratory behaviors (Figure 6a). Specifically, blue whale vocalizations appeared earlier in the season but over a shorter period, peaking between July and October, whereas fin whale call detections started later and persisted longer, spanning from August to the following April. In addition to seasonal variability, both species exhibited notable interannual variability in call activity, with fin whale detections showing a slightly increasing trend and blue whale showing a significant decline after 2022 (Ryan et al., 2025). To validate these seasonal and annual distributions, we compared DASNet detections with independent records from the Monterey Accelerated Research System (MARS) hydrophone (Figure 6a). Despite differences in sensing modality, spatial coverage, and detection criteria, the two systems yielded highly consistent seasonal peaks during overlapping time windows, supporting the robustness of DAS-based passive acoustic monitoring.

In addition to detecting whale vocalizations, DASNet provides precise arrival-time estimates for individual calls, enabling automatic source localization. We localized detected whale calls using a grid-based approach that minimizes the L1 misfit between theoretical and model-predicted arrival times (Xiao et al., 2025), assuming a nominal source depth of 15 m (Stimpert et al., 2015) and a constant water velocity (Figure 6c). Most localized calls cluster near the continental shelf slopes (Figure 6b and Figure S7), consistent with previous studies suggesting that such topographic features enhance biological productivity through upwelling, mixing, and nutrient retention, creating energetically favorable foraging habitats that attract baleen whales (Moors-Murphy, 2014). Note that the spatial density of localizations is also influenced by the detection sensitivity of the DAS cable and the limitations of the localization algorithm, which provides weaker constraints in the direction perpendicular to the cable (Figure 6c). Therefore, the localization heatmap should be interpreted as a convolution of true biological activity and observation constraints. These results demonstrate that the DAS infrastructure, paired with automatic detection capabilities of DASNet, offers a promising approach for large-scale, long-duration monitoring of marine mammal distribution.

Besides ecological observations, DASNet can also support the monitoring of anthropogenic acoustic sources, such as vessel traffic, which poses growing threats to baleen whales through acoustic masking, habitat displacement, and ship strikes (Council et al., 2003; McDonald et al., 2006). Although vessel noise typically lacks clear arrivals, DASNet detects these continuous acoustic signals through its bounding-box predictions. Combining these detections with a beamforming-inspired migration approach (Paap et al., 2025), we can estimate the spatial trajectories of moving vessels. As a demonstration, we analyzed a two-hour DAS recording from April 7, 2023, during which a vessel with available automatic identification system (AIS) data passed near the SeaFOAM cable. DASNet detected 127 vessel signal segments, and the inferred locations traced a coherent trajectory that closely matches the vessel’s movement as recorded by AIS (Figure 7). As with whale vocalizations, localization ambiguity inherent to the linear array geometry remains a challenge, producing mirror-image solutions on both sides of the cable. This limitation can be mitigated by deploying curved cable geometries or supplemental arrays. The ability to track vessels alongside whale calls positions DAS as a multi-purpose tool for integrated monitoring of marine ecosystems and the human activities that affect them.

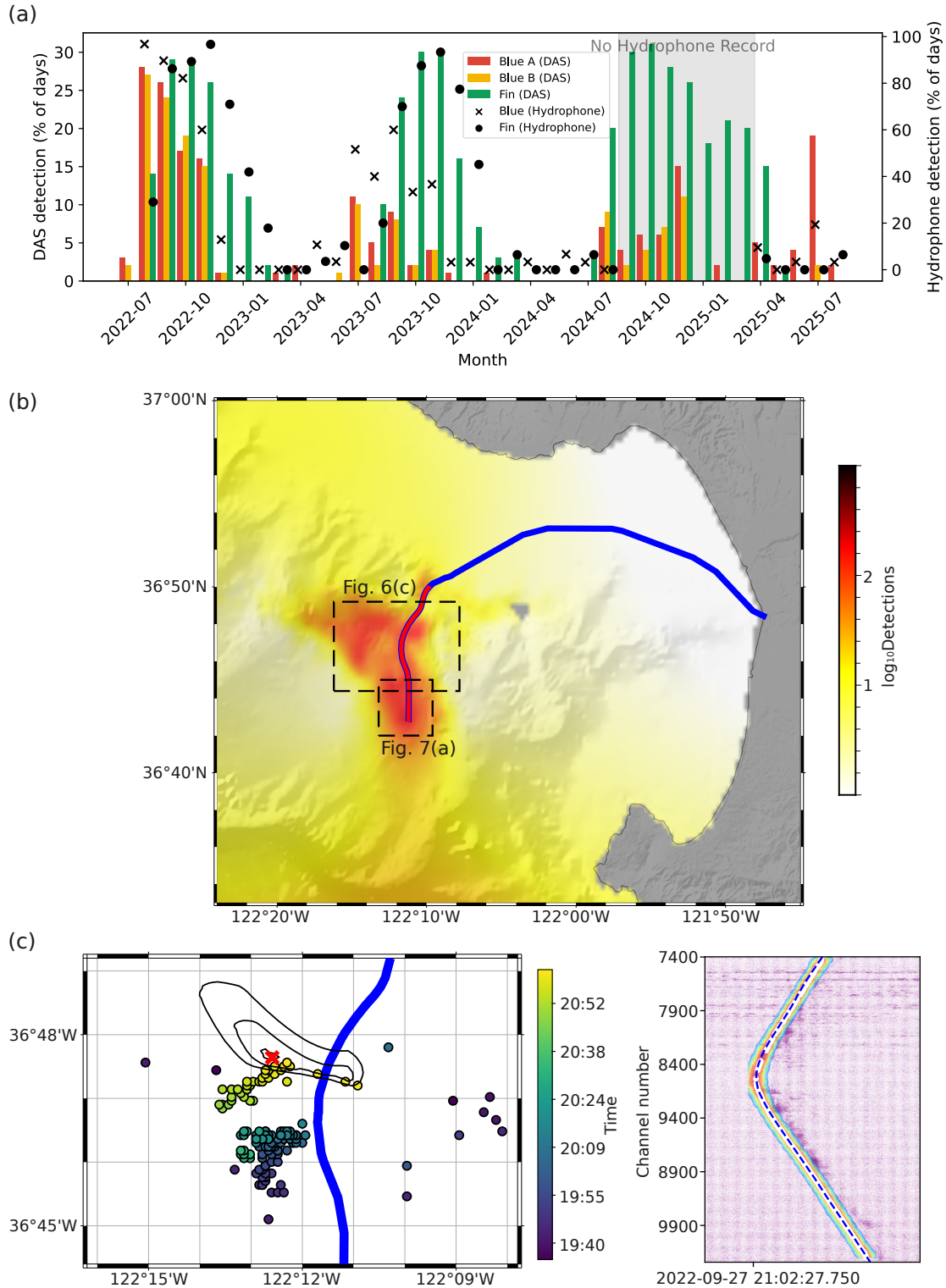


Figure 6: Whale call detection and localization. (a) Monthly occurrence of DAS-detected fin whale calls and blue whale A and B calls, reported as the percentage of days per month with detections. A day is counted as having a DAS detection if whale calls occupy $>3\%$ of the day; for the MBARI hydrophone catalog, a day is counted when the daily Call Index exceeds 1.05 (see Figure S6). (b) Spatial distribution of all fin whale calls localized over the three-year record. Results far from the cable should be interpreted with caution due to limitations of cable geometry and instrument sensitivity. (c) Case study spanning approximately 2 h. The left panel shows locations of 148 calls detected during this interval; the red cross marks the call whose waveform is shown at right. Black concentric contours denote misfit levels of 0.1 s, 0.2 s, and 0.3 s. In the right panel, the white curve traces arrival-time picks extracted from the model's probabilistic mask, and the blue curve shows the predicted arrival-time curve computed from the estimated source location.

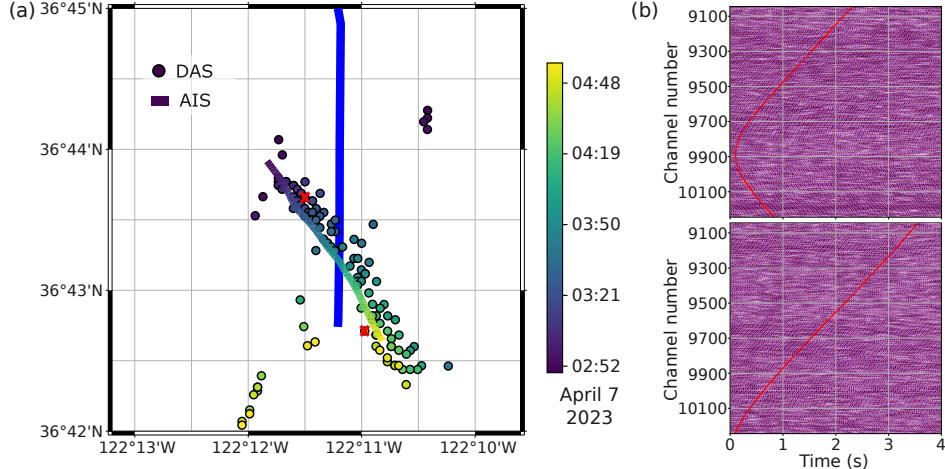


Figure 7: (a) Locations of vessel signals detected by DAS on April 7, 2023. Estimated source positions closely match AIS-reported vessel locations. Note that mirror-image solutions appear on both the east and west sides of the cable, reflecting the inherent left-right ambiguity of a near-linear array. The blue vertical line indicates the DAS cable. (b) Two signal segments corresponding to the red cross positions in (a), and the predicted arrival curve based on the localization results is marked with red curves.

4 Discussion

DAS provides a unique opportunity to observe the ocean as a coupled system over spatial scales from meters to tens of kilometers and temporal scales from seconds to seasons. Prior DAS studies commonly addressed individual processes in isolation, such as detecting earthquakes, tracking whale calls, or monitoring vessel traffic, requiring separate workflows with distinct preprocessing steps and manual inspection. In this work, we have developed DASNet, a unified instance-segmentation framework that reformulates DAS analysis around event-centric representations. Instead of interpreting continuous wavefields channel by channel, DASNet identifies each event as an individual spatiotemporal instance, predicting bounding boxes, arrival-time masks, and class labels for downstream scientific analyses. The unified framework enables a single DAS array to function as a multi-purpose observatory capable of distinguishing diverse signal sources. It supports local and regional earthquake detection and localization, identification and azimuthal characterization of distant T-wave sources, systematic monitoring and tracking of baleen whale vocalizations, and localization of nearby vessel traffic.

The reliability of automated event detection and classification is central to the interpretation of large-scale DAS observations. We evaluated the performance of DASNet on datasets constructed through a semi-supervised refinement process. The results indicate that DASNet achieves consistently high detection performance for well-represented signal classes and maintains stable behavior on continuous data. Comparisons with independent seismic catalogs, hydrophone-based whale call records, and vessel tracking data further support the validity of the detected events, demonstrating that the automated predictions are broadly consistent with established observational systems. These cross-validation results provide confidence that the extracted event catalogs capture physically meaningful signals rather than spurious detections.

Accurate and consistent arrival-time measurements are equally important for quantitative analyses such as event localization and subsurface imaging. Across the evaluated signal classes, DASNet achieves arrival-time precision adequate for the applications demonstrated in this study, though seismic phases exhibit slightly reduced timing precision relative to impulsive acoustic signals. The reduced precision for seismic phases likely reflects the inherent difficulty of manual phase picking in DAS records rather than a fundamental limitation of the approach. Emergent onsets or lower-SNR events make it difficult for human annotators to place consistent picks, introducing label variability that affects both training and evaluation. Moreover, the model-derived picks tend to be slightly earlier than manual annotations, suggesting that the model may be sensitive to subtle onset features that are difficult to identify consistently by visual inspection.

Operational deployment of event-centric DAS analysis further requires computational efficiency and sta-

bility on continuous data streams. Benchmarking on three months of continuous SeaFOAM data (2024-08 to 2024-10), one of the most event-dense periods in our observations, shows that the inference time per 60 s-segment rarely exceeds 0.5 s on a standard Google Cloud GPU instance with 8 vCPUs and an NVIDIA T4 GPU, which is sufficiently efficient for real-time monitoring of diverse seismic and acoustic events (Figure S8). Because DASNet employs a two-stage architecture (see Methods), the second-stage branches for classification, bounding-box regression, and mask generation require additional computation when the number of detected instances increases. However, individual 60 s segments in the SeaFOAM dataset rarely contain fifteen or more distinct signals, so the overall two-stage overhead remains limited under typical operating conditions.

Despite these capabilities, several challenges remain. One limitation of DASNet is that the current training dataset does not yet encompass the full diversity of signal types present in continuous DAS recordings. As a result, certain signal classes that are either previously unrecognized or represent atypical variants of known types remain difficult to detect. Signals outside the training distribution may also be assigned to the most similar known classes by the model, because many signal types share common characteristics relative to background noise. One example is a category of signals that may represent candidate T-waves from the North Pacific (Figure S9). These signals often exhibit reduced coherence and less distinct moveout patterns compared with the more commonly observed T-waves, potentially reflecting generation in shallower water and enhanced scattering along complex propagation paths. Because their classification remains uncertain and representative examples were limited, these signals were not included in the current training set. However, an important advantage of the DASNet framework is its ability to support rapid iterative expansion through semi-supervised learning (see Methods). Once emerging or ambiguously classified signal types are identified and verified, a small number of representative examples can be incorporated into the training set and propagated through successive refinement cycles. This semi-supervised learning process provides an effective approach for continuously improving monitoring coverage as new signal types are recognized.

Another challenge is generalization across arrays. DASNet in this study was trained on SeaFOAM data, and performance can degrade when applied to cables with different coupling conditions, noise characteristics, or spatial sampling. Although the architecture supports inputs of varying sizes, direct application to substantially larger or smaller arrays without additional adaptation or fine-tuning has not been evaluated. Potential directions to enhance model generalization include data augmentation that simulates various DAS configurations, including spatial and temporal resampling, adding realistic noise, and composing new inputs through cropping and stitching (Zhu et al., 2020), as well as semi-supervised fine-tuning on the target datasets. We did not adopt a fully automated self-training loop in this study, because small errors in pseudo-labels can accumulate and bias the model, but recent work has shown that when the base model is sufficiently accurate, iterative self-training can approach full automation (Kirillov et al., 2023). As DAS datasets continue to grow in volume and diversity, developing robust strategies for model adaptation across different cable configurations and geological settings will be critical for ensuring the reliability and scalability of DAS-based monitoring and analysis.

In conclusion, DASNet transforms distributed acoustic sensing from a set of task-specific pipelines into a unified event-level observatory capable of simultaneously monitoring seismic activity, marine ecosystems, and anthropogenic noise along the same fiber. It enables the simultaneous detection and analysis of diverse signals, including earthquakes, T-waves, whale vocalizations, and vessel activity, thereby supporting long-term monitoring of multiple ocean processes using a single DAS array while maintaining the computational efficiency required for continuous real-time operation. These results demonstrate that combining DAS with deep learning provides scalable, high-resolution monitoring of marine environments using existing telecommunications infrastructure. In regions where conventional seismic and bioacoustic instruments remain sparse or absent, expanding submarine DAS coverage could substantially enhance observational capability. Although further developments are needed to ensure robust generalization across diverse DAS arrays, this study provides a foundation for large-scale ocean monitoring through the integration of fiber-optic sensing and deep learning.

Acknowledgments

We thank Wenbo Wu and John Ryan for helpful discussions and suggestions on marine acoustic analysis. We thank Martin Karrenbach and Victor Yartsev of OptaSense Inc. for their assistance in installing and configuring the monterey bay distributed acoustic sensing equipment. This work was supported by the National Science Foundation (NSF) under Grant No. OCE-2023301 and by the California Governor’s Office of Emergency Services under Agreement No. 6172-2018. This work was also supported by the EPIC (Electric Program Investment Charge) program of the California Energy Commission (CEC) to Lawrence Berkeley National Laboratory.

References

- Adeniyi, B. A., Abdul Latiff, A. H., Adedeji, Z. O., Md Arshad, A. R., & Asfha, D. T. (2025). Directional sensitivity of fibre optic cables for surface seismic reflection distributed acoustic sensing: A review and potential solutions for enhanced sensitivity. *Geomechanics and Geophysics for Geo-Energy and Geo-Resources*, *11*(1), 60.
- Ahonen, H., Stafford, K. M., Lydersen, C., Berchok, C. L., Moore, S. E., & Kovacs, K. M. (2021). Interannual variability in acoustic detection of blue and fin whale calls in the northeast atlantic high arctic between 2008 and 2018. *Endangered Species Research*, *45*, 209–224.
- Au, W. W., & Hastings, M. C. (2008). *Principles of marine bioacoustics* (Vol. 510). Springer.
- Barlow, D. R., Klinck, H., Ponirakis, D., Branch, T. A., & Torres, L. G. (2023). Environmental conditions and marine heatwaves influence blue whale foraging and reproductive effort. *Ecology and Evolution*, *13*(2), e9770.
- Biondi, E., Zhu, W., Li, J., Williams, E. F., & Zhan, Z. (2023). An upper-crust lid over the long valley magma chamber. *Science Advances*, *9*(42), eadi9878.
- Boitz, N., & Shapiro, S. (2024). Detection of microseismic events in continuous das data using convolutional neural networks. *The Leading Edge*, *43*(1), 16–22.
- Bouffaut, L., Taweesintanon, K., Kriesell, H. J., Rørstadbotnen, R. A., Potter, J. R., Landrø, M., . . . others (2022). Eavesdropping at the speed of light: Distributed acoustic sensing of baleen whales in the arctic. *Frontiers in Marine Science*, *9*, 901348.
- Carvajal, M., Sepúlveda, I., Gubler, A., & Garreaud, R. (2022). Worldwide signature of the 2022 tonga volcanic tsunami. *Geophysical Research Letters*, *49*(6), e2022GL098153.
- Council, N. R., on Earth, D., Studies, L., Board, O. S., & on Potential Impacts of Ambient Noise in the Ocean on Marine Mammals, C. (2003). Ocean noise and marine mammals.
- Ding, Q., Shen, Z., Zhu, W., & Liu, B. (2025). Dasformer: self-supervised pretraining for earthquake monitoring. *Visual Intelligence*, *3*(1), 14.
- Dosovitskiy, A. (2020). An image is worth 16x16 words: Transformers for image recognition at scale. *arXiv preprint arXiv:2010.11929*.
- Dziak, R., Bohnenstiehl, D., Matsumoto, H., Fox, C., Smith, D., Tolstoy, M., . . . Fowler, M. (2004). P-and t-wave detection thresholds, pn velocity estimate, and detection of lower mantle and core p-waves on ocean sound-channel hydrophones at the mid-atlantic ridge. *Bulletin of the Seismological Society of America*, *94*(2), 665–677.
- Eguíluz, V. M., Fernández-Gracia, J., Irigoien, X., & Duarte, C. M. (2016). A quantitative assessment of arctic shipping in 2010–2014. *Scientific reports*, *6*(1), 30682.
- Erbe, C., Marley, S. A., Schoeman, R. P., Smith, J. N., Trigg, L. E., & Embling, C. B. (2019). The effects of ship noise on marine mammals—a review. *Frontiers in Marine Science*, *6*, 606.

- Fernández-Ruiz, M. R., Martins, H. F., Williams, E. F., Becerril, C., Magalhães, R., Costa, L., . . . González-Herráez, M. (2022). Seismic monitoring with distributed acoustic sensing from the near-surface to the deep oceans. *Journal of Lightwave Technology*, *40*(5), 1453–1463.
- Fox, C. G., Matsumoto, H., & Lau, T.-K. A. (2001). Monitoring pacific ocean seismicity from an autonomous hydrophone array. *Journal of Geophysical Research: Solid Earth*, *106*(B3), 4183–4206.
- Goestchel, Q., Wilcock, W. S., & Abadi, S. (2025). Enhancing fin whale vocalizations in distributed acoustic sensing data. *The Journal of the Acoustical Society of America*, *157*(5), 3655–3666.
- Gou, Y., Allen, R. M., Zhu, W., Taira, T., & Chen, L.-W. (2025). Leveraging submarine das arrays for offshore earthquake early warning: A case study in monterey bay, california. *Bulletin of the Seismological Society of America*, *115*(2), 516–532.
- Hanson, J. A., & Bowman, J. R. (2006). Methods for monitoring hydroacoustic events using direct and reflected t waves in the indian ocean. *Journal of Geophysical Research: Solid Earth*, *111*(B2).
- Harbitz, C. B., Løvholt, F., Pedersen, G., & Masson, D. G. (2006). Mechanisms of tsunami generation by submarine landslides: a short review. *Norwegian Journal of Geology/Norsk Geologisk Forening*, *86*(3).
- He, K., Gkioxari, G., Dollár, P., & Girshick, R. (2017). Mask r-cnn. In *Proceedings of the ieee international conference on computer vision* (pp. 2961–2969).
- He, K., Zhang, X., Ren, S., & Sun, J. (2016). Deep residual learning for image recognition. In *Proceedings of the ieee conference on computer vision and pattern recognition* (pp. 770–778).
- Hildebrand, J. A. (2009). Anthropogenic and natural sources of ambient noise in the ocean. *Marine Ecology Progress Series*, *395*, 5–20.
- Huot, F., Lellouch, A., Given, P., Luo, B., Clapp, R. G., Nemeth, T., . . . Biondi, B. L. (2022). Detection and characterization of microseismic events from fiber-optic das data using deep learning. *Seismological Society of America*, *93*(5), 2543–2553.
- Ide, S., Araki, E., & Matsumoto, H. (2021). Very broadband strain-rate measurements along a submarine fiber-optic cable off cape muroto, nankai subduction zone, japan. *Earth, Planets and Space*, *73*(1), 1–10.
- Kanamori, H. (1972). Mechanism of tsunami earthquakes. *Physics of the earth and planetary interiors*, *6*(5), 346–359.
- Kirillov, A., Mintun, E., Ravi, N., Mao, H., Rolland, C., Gustafson, L., . . . others (2023). Segment anything. In *Proceedings of the ieee/cvf international conference on computer vision* (pp. 4015–4026).
- Landrø, M., Bouffaut, L., Kriesell, H. J., Potter, J. R., Rørstadbotnen, R. A., Taweessintananon, K., . . . others (2022). Sensing whales, storms, ships and earthquakes using an arctic fibre optic cable. *Scientific Reports*, *12*(1), 19226.
- Lavery, T. J., Roudnew, B., Seymour, J., Mitchell, J. G., Smetacek, V., & Nicol, S. (2014). Whales sustain fisheries: blue whales stimulate primary production in the southern ocean. *Marine Mammal Science*, *30*(3), 888–904.
- Lindsey, N. J., Dawe, T. C., & Ajo-Franklin, J. B. (2019). Illuminating seafloor faults and ocean dynamics with dark fiber distributed acoustic sensing. *Science*, *366*(6469), 1103–1107.
- Lindsey, N. J., & Martin, E. R. (2021). Fiber-optic seismology. *Annual Review of Earth and Planetary Sciences*, *49*(1), 309–336.
- Lindsey, N. J., Rademacher, H., & Ajo-Franklin, J. B. (2020). On the broadband instrument response of fiber-optic das arrays. *Journal of Geophysical Research: Solid Earth*, *125*(2), e2019JB018145.

- Lior, I., Mercerat, E. D., Rivet, D., Sladen, A., & Ampuero, J.-P. (2022). Imaging an underwater basin and its resonance modes using optical fiber distributed acoustic sensing. *Seismological Society of America*, *93*(3), 1573–1584.
- Lior, I., Sladen, A., Rivet, D., Ampuero, J.-P., Hello, Y., Becerril, C., ... others (2021). On the detection capabilities of underwater distributed acoustic sensing. *Journal of Geophysical Research: Solid Earth*, *126*(3), e2020JB020925.
- Lipovsky, B. P. (2024). Rapid: Multiplexed distributed acoustic sensing (das) at the ocean observatory initiative (ooi) regional cabled array (rca). *NSF Award Number 2415521. Directorate for Geosciences*, *24*(2415521), 15521.
- Liu, Z., Lin, Y., Cao, Y., Hu, H., Wei, Y., Zhang, Z., ... Guo, B. (2021). Swin transformer: Hierarchical vision transformer using shifted windows. In *Proceedings of the ieee/cvf international conference on computer vision* (pp. 10012–10022).
- Liu, Z., Mao, H., Wu, C.-Y., Feichtenhofer, C., Darrell, T., & Xie, S. (2022). A convnet for the 2020s. In *Proceedings of the ieee/cvf conference on computer vision and pattern recognition* (pp. 11976–11986).
- Lv, H., Zeng, X., Chi, B., Zhang, G., & Thurber, C. (2023). Monitoring seismicity triggered by geothermal site shutdown with a surface das array at brady hot springs. *Geophysical Journal International*, *235*(2), 1861–1871.
- Ma, Y., Eaton, D., Igonin, N., & Wang, C. (2023). Machine learning-assisted processing workflow for multi-fiber das microseismic data. *Frontiers in Earth Science*, *11*, 1096212.
- McDonald, M. A., Hildebrand, J. A., & Webb, S. C. (1995). Blue and fin whales observed on a seafloor array in the northeast pacific. *The Journal of the Acoustical Society of America*, *98*(2), 712–721.
- McDonald, M. A., Hildebrand, J. A., & Wiggins, S. M. (2006). Increases in deep ocean ambient noise in the northeast pacific west of san nicolas island, california. *The Journal of the Acoustical Society of America*, *120*(2), 711–718.
- Miao, Y., Rabade, S., Liu, M., & Spica, Z. J. (2025). Evaluating subsurface imaging performance with ocean-bottom distributed acoustic sensing and double beamforming. *Geophysical Journal International*, *242*(2), ggaf190.
- Moors-Murphy, H. B. (2014). Submarine canyons as important habitat for cetaceans, with special reference to the gully: a review. *Deep Sea Research Part II: Topical Studies in Oceanography*, *104*, 6–19.
- Mousavi, S. M., Ellsworth, W. L., Zhu, W., Chuang, L. Y., & Beroza, G. C. (2020). Earthquake transformer—an attentive deep-learning model for simultaneous earthquake detection and phase picking. *Nature communications*, *11*(1), 3952.
- Muir, J. B., & Zhan, Z. (2022). Wavefield-based evaluation of das instrument response and array design. *Geophysical Journal International*, *229*(1), 21–34.
- Näsholm, S. P., Iranpour, K., Wuestefeld, A., Dando, B. D., Baird, A. F., & Oye, V. (2022). Array signal processing on distributed acoustic sensing data: Directivity effects in slowness space. *Journal of Geophysical Research: Solid Earth*, *127*(2), e2021JB023587.
- Oestreich, W. K., Abrahms, B., McKenna, M. F., Goldbogen, J. A., Crowder, L. B., & Ryan, J. P. (2022). Acoustic signature reveals blue whales tune life-history transitions to oceanographic conditions. *Functional Ecology*, *36*(4), 882–895.
- Oestreich, W. K., Fahlbusch, J. A., Cade, D. E., Calambokidis, J., Margolina, T., Joseph, J., ... others (2020). Animal-borne metrics enable acoustic detection of blue whale migration. *Current Biology*, *30*(23), 4773–4779.

- Oestreich, W. K., Oliver, R. Y., Chapman, M. S., Go, M., & McKenna, M. F. (2024). Listening to animal behavior to understand changing ecosystems. *Trends in Ecology & Evolution*.
- Omira, R., Ramalho, R., Kim, J., González, P. J., Kadri, U., Miranda, J., ... Baptista, M. (2022). Global tonga tsunami explained by a fast-moving atmospheric source. *Nature*, *609*(7928), 734–740.
- Paap, B., Vandeweyer, V., van Wees, J.-D., & Kraaijpoel, D. (2025). Leveraging distributed acoustic sensing for monitoring vessels using submarine fiber-optic cables. *Applied Ocean Research*, *154*, 104422.
- Paitz, P., Edme, P., Gräff, D., Walter, F., Doetsch, J., Chalari, A., ... Fichtner, A. (2021). Empirical investigations of the instrument response for distributed acoustic sensing (das) across 17 octaves. *Bulletin of the Seismological Society of America*, *111*(1), 1–10.
- Parnell-Turner, R., Smith, D., & Dziak, R. (2022). Hydroacoustic monitoring of seafloor spreading and transform faulting in the equatorial atlantic ocean. *Journal of Geophysical Research: Solid Earth*, *127*(7), e2022JB024008.
- Payne, R., & Webb, D. (1971). Orientation by means of long range acoustic signaling in baleen whales. *Annals of the New York Academy of Sciences*, *188*(1), 110–141.
- Payne, R. S., & McVay, S. (1971). Songs of humpback whales: Humpbacks emit sounds in long, predictable patterns ranging over frequencies audible to humans. *Science*, *173*(3997), 585–597.
- Richardson, W. J., Greene Jr, C. R., Malme, C. I., & Thomson, D. H. (2013). *Marine mammals and noise*. Academic press.
- Rivet, D., Baillet, M., Trabattoni, A., Van Den Ende, M., Chèze, J., Maron, C., ... Epos-France (2025). *Three underwater fiber-optic cables offshore of central chile*. Epos-France Seismological Data Centre. doi: 10.15778/RESIF.F1
- Roman, J., Estes, J. A., Morissette, L., Smith, C., Costa, D., McCarthy, J., ... Smetacek, V. (2014). Whales as marine ecosystem engineers. *Frontiers in Ecology and the Environment*, *12*(7), 377–385.
- Romanowicz, B., Allen, R., Brekke, K., Chen, L.-W., Gou, Y., Henson, I., ... others (2023). Seafoam: A year-long das deployment in monterey bay, california. *Seismological Research Letters*, *94*(5), 2348–2359.
- Ross, Z. E., Yue, Y., Meier, M.-A., Hauksson, E., & Heaton, T. H. (2019). Phaselink: A deep learning approach to seismic phase association. *Journal of Geophysical Research: Solid Earth*, *124*(1), 856–869.
- Ryan, J. P., Benoit-Bird, K. J., Oestreich, W. K., Leary, P., Smith, K. B., Waluk, C. M., ... others (2022). Oceanic giants dance to atmospheric rhythms: Ephemeral wind-driven resource tracking by blue whales. *Ecology letters*, *25*(11), 2435–2447.
- Ryan, J. P., Oestreich, W. K., Benoit-Bird, K. J., Waluk, C. M., Rueda, C. A., Cline, D. E., ... others (2025). Audible changes in marine trophic ecology: Baleen whale song tracks foraging conditions in the eastern north pacific. *Plos one*, *20*(2), e0318624.
- Saw, J., Luo, L., Chu, K., Ryan, J., Soga, K., & Wu, Y. (2025). Distributed acoustic sensing for whale vocalization monitoring: A vertical deployment field test. *Seismological Research Letters*, *96*(2A), 801–815.
- Seike, K., Shirai, K., & Kogure, Y. (2013). Disturbance of shallow marine soft-bottom environments and megabenthos assemblages by a huge tsunami induced by the 2011 m9. 0 tohoku-oki earthquake. *PLoS One*, *8*(6), e65417.
- Shen, J., & Zhu, T. (2026). Unsupervised characterization of rain-induced seismic noise in urban fiber-optic networks using deep embedded clustering. *Water Resources Research*, *62*(1), e2025WR041137.
- Shen, Z., & Wu, W. (2024). Ocean bottom distributed acoustic sensing for oceanic seismicity detection and seismic ocean thermometry. *Journal of Geophysical Research: Solid Earth*, *129*(3), e2023JB027799.

- Shi, Q., Williams, E. F., Lipovsky, B. P., Denolle, M. A., Wilcock, W. S., Kelley, D. S., & Schoedl, K. (2024). Multiplexed distributed acoustic sensing offshore central oregon. *Authorea Preprints*.
- Simon, M., Stafford, K. M., Beedholm, K., Lee, C. M., & Madsen, P. T. (2010). Singing behavior of fin whales in the davis strait with implications for mating, migration and foraging. *The Journal of the Acoustical Society of America*, *128*(5), 3200–3210.
- Širović, A., Hildebrand, J. A., & Wiggins, S. M. (2007). Blue and fin whale call source levels and propagation range in the southern ocean. *The Journal of the Acoustical Society of America*, *122*(2), 1208–1215.
- Sladen, A., Rivet, D., Ampuero, J. P., De Barros, L., Hello, Y., Calbris, G., & Lamare, P. (2019). Distributed sensing of earthquakes and ocean-solid earth interactions on seafloor telecom cables. *Nature communications*, *10*(1), 5777.
- Smith, D. K., Tolstoy, M., Fox, C. G., Bohnenstiehl, D. R., Matsumoto, H., & J. Fowler, M. (2002). Hydroacoustic monitoring of seismicity at the slow-spreading mid-atlantic ridge. *Geophysical Research Letters*, *29*(11), 13–1.
- Stimpert, A. K., DeRuiter, S. L., Falcone, E. A., Joseph, J., Douglas, A. B., Moretti, D. J., . . . others (2015). Sound production and associated behavior of tagged fin whales (*balaenoptera physalus*) in the southern california bight. *Animal Biotelemetry*, *3*(1), 23.
- Suetsugu, D., & Shiobara, H. (2014). Broadband ocean-bottom seismology. *Annual Review of Earth and Planetary Sciences*, *42*(1), 27–43.
- Sun, H., Ross, Z. E., Zhu, W., & Azzadenesheli, K. (2023). Phase neural operator for multi-station picking of seismic arrivals. *Geophysical Research Letters*, *50*(24), e2023GL106434.
- Tepp, G., & Dziak, R. P. (2021). The seismo-acoustics of submarine volcanic eruptions. *Journal of Geophysical Research: Solid Earth*, *126*(4), e2020JB020912.
- Thomsen, M. S., Mondardini, L., Thorat, F., Gerber, D., Montie, S., South, P. M., . . . Schiel, D. R. (2021). Cascading impacts of earthquakes and extreme heatwaves have destroyed populations of an iconic marine foundation species. *Diversity and Distributions*, *27*(12), 2369–2383.
- Tolstoy, I., & Ewing, M. (1950). The t phase of shallow-focus earthquakes. *Bulletin of the Seismological Society of America*, *40*(1), 25–51.
- Tonegawa, T., & Araki, E. (2024). High-frequency tsunamis excited near torishima island, japan, observed by distributed acoustic sensing. *Geophysical Research Letters*, *51*(11), e2024GL108714.
- Toomey, D. R., Allen, R. M., Barclay, A. H., Bell, S. W., Bromirski, P. D., Carlson, R. L., . . . others (2014). The cascadia initiative: A sea change in seismological studies of subduction zones. *Oceanography*, *27*(2), 138–150.
- Trafford, A., Ellwood, R., Wacquier, L., Godfrey, A., Minto, C., Coughlan, M., & Donohue, S. (2022). Distributed acoustic sensing for active offshore shear wave profiling. *Scientific Reports*, *12*(1), 9691.
- Tyack, P. L. (2008). Implications for marine mammals of large-scale changes in the marine acoustic environment. *Journal of Mammalogy*, *89*(3), 549–558.
- Van den Ende, M., Lior, I., Ampuero, J.-P., Sladen, A., Ferrari, A., & Richard, C. (2021). A self-supervised deep learning approach for blind denoising and waveform coherence enhancement in distributed acoustic sensing data. *IEEE Transactions on Neural Networks and Learning Systems*, *34*(7), 3371–3384.
- van den Ende, M. P., & Ampuero, J.-P. (2021). Evaluating seismic beamforming capabilities of distributed acoustic sensing arrays. *Solid Earth*, *12*(4), 915–934.
- Wang, H. F., Zeng, X., Miller, D. E., Fratta, D., Feigl, K. L., Thurber, C. H., & Mellors, R. J. (2018). Ground motion response to an ml 4.3 earthquake using co-located distributed acoustic sensing and seismometer arrays. *Geophysical Journal International*, *213*(3), 2020–2036.

- Wech, A., Tepp, G., Lyons, J., & Haney, M. (2018). Using earthquakes, t waves, and infrasound to investigate the eruption of bogoslof volcano, alaska. *Geophysical Research Letters*, *45*(14), 6918–6925.
- Wiggins, S. M., Oleson, E. M., McDonald, M. A., & Hildebrand, J. A. (2005). Blue whale (*balaenoptera musculus*) diel call patterns offshore of southern california. *Aquatic Mammals*, *31*(2), 161.
- Wilcock, W. S., Abadi, S., & Lipovsky, B. P. (2023). Distributed acoustic sensing recordings of low-frequency whale calls and ship noise offshore central oregon. *JASA Express Letters*, *3*(2).
- Williams, E. F., Fernández-Ruiz, M. R., Magalhaes, R., Vanthillo, R., Zhan, Z., González-Herráez, M., & Martins, H. F. (2019). Distributed sensing of microseisms and teleseisms with submarine dark fibers. *Nature communications*, *10*(1), 5778.
- Williams, E. F., Zhan, Z., Martins, H. F., Fernández-Ruiz, M. R., Martín-López, S., González-Herráez, M., & Callies, J. (2022). Surface gravity wave interferometry and ocean current monitoring with ocean-bottom das. *Journal of Geophysical Research: Oceans*, *127*(5), e2021JC018375.
- Wu, W., Zhan, Z., Peng, S., Ni, S., & Callies, J. (2020). Seismic ocean thermometry. *Science*, *369*(6510), 1510–1515.
- Wuestefeld, A., Spica, Z. J., Aderhold, K., Huang, H.-H., Ma, K.-F., Lai, V. H., ... others (2024). The global das month of february 2023. *Seismological Research Letters*, *95*(3), 1569–1577.
- Xenaki, A., Gerstoft, P., Williams, E., & Abadi, S. (2025). Overview of distributed acoustic sensing: Theory and ocean applications. *The Journal of the Acoustical Society of America*, *158*(1), 801–825.
- Xiao, H., Spica, Z. J., Li, J., & Zhan, Z. (2024). Detection of earthquake infragravity and tsunami waves with underwater distributed acoustic sensing. *Geophysical Research Letters*, *51*(2), e2023GL106767.
- Xiao, H., Tilmann, F., van den Ende, M., Rivet, D., Loureiro, A., Tsuji, T., ... Denolle, M. A. (2026, 02). Deepsubdas: an earthquake phase picker from submarine distributed acoustic sensing data. *Geophysical Journal International*, *245*(2), ggag061. Retrieved from <https://doi.org/10.1093/gji/ggag061> doi: 10.1093/gji/ggag061
- Xiao, H., Zhang, S., Moss, R., & Zhan, Z. (2025). Imaging underwater faults and tracking whales with optical fiber sensing. *Seismological Research Letters*, *96*(2A), 678–690.
- Yin, J., Zhu, W., Li, J., Biondi, E., Miao, Y., Spica, Z. J., ... others (2023). Earthquake magnitude with das: A transferable data-based scaling relation. *Geophysical Research Letters*, *50*(10), e2023GL103045.
- Yu, P., Zhu, T., Marone, C., Elsworth, D., & Yu, M. (2024). Daseventnet: Ai-based microseismic detection on distributed acoustic sensing data from the utah forge well 16a (78)-32 hydraulic stimulation. *Journal of Geophysical Research: Solid Earth*, *129*(9), e2024JB029102.
- Yu, S., Ma, J., & Wang, W. (2019). Deep learning for denoising. *Geophysics*, *84*(6), V333–V350.
- Zhan, Z. (2020). Distributed acoustic sensing turns fiber-optic cables into sensitive seismic antennas. *Seismological Research Letters*, *91*(1), 1–15.
- Zhang, M., Ellsworth, W. L., & Beroza, G. C. (2019). Rapid earthquake association and location. *Seismological Research Letters*, *90*(6), 2276–2284.
- Zhu, W., & Beroza, G. C. (2019). Phasenet: a deep-neural-network-based seismic arrival-time picking method. *Geophysical Journal International*, *216*(1), 261–273.
- Zhu, W., Biondi, E., Li, J., Yin, J., Ross, Z. E., & Zhan, Z. (2023). Seismic arrival-time picking on distributed acoustic sensing data using semi-supervised learning. *Nature Communications*, *14*(1), 8192.
- Zhu, W., McBrearty, I. W., Mousavi, S. M., Ellsworth, W. L., & Beroza, G. C. (2022). Earthquake phase association using a bayesian gaussian mixture model. *Journal of Geophysical Research: Solid Earth*, *127*(5), e2021JB023249.

- Zhu, W., Mousavi, S. M., & Beroza, G. C. (2019). Seismic signal denoising and decomposition using deep neural networks. *IEEE Transactions on Geoscience and Remote Sensing*, 57(11), 9476–9488.
- Zhu, W., Mousavi, S. M., & Beroza, G. C. (2020). Seismic signal augmentation to improve generalization of deep neural networks. In *Advances in geophysics* (Vol. 61, pp. 151–177). Elsevier.
- Zhu, W., Tai, K. S., Mousavi, S. M., Bailis, P., & Beroza, G. C. (2022). An end-to-end earthquake detection method for joint phase picking and association using deep learning. *Journal of Geophysical Research: Solid Earth*, 127(3), e2021JB023283.

Supplementary Information

A deep learning framework for marine acoustic and seismic monitoring with distributed acoustic sensing

Chun Zhang^{1,2}, Weiqiang Zhu^{1,2}, Barbara A. Romanowicz^{1,2}, Richard M Allen^{1,2}, Kenichi Soga³, and Yuxin Wu⁴

¹Department of Earth & Planetary Science, University of California, Berkeley

²Berkeley Seismology Laboratory, University of California, Berkeley

³Department of Civil & Environmental Engineering, University of California, Berkeley

⁴Earth and Environmental Sciences Area, Lawrence Berkeley National Laboratory

The Supplementary Information provides additional analyses and validation results that support the main conclusions of this study. It includes a detailed description of the DASNet architecture (Text S1). We also provide spectrograms of representative channel records for each major signal type corresponding to the examples shown in the main text (Figure S1). Additional comparisons of DASNet detections under different confidence thresholds are presented in Figure S2. Further earthquake location results only based on DAS phase arrivals are shown in Figure S3, together with extended analyses of array geometry effects on T-wave azimuthal resolution (Figure S4). We also present examples from independent DAS and hydrophone datasets, including T-wave observations from the OOI Regional Cabled Array (Figure S5), the whale Call Index (CI) from the MBARI hydrophone (Figure S6), and blue whale detections from the SeaFOAM DAS array (Figure S7), demonstrating the generality of the proposed approach. Inference-time statistics (Figure S8) are further provided to evaluate the computational efficiency of DASNet under varying detection scenarios. Finally, we show an example of a poorly structured T-wave-like signal from the high-latitude North Pacific (Figure S9), illustrating a type of signal variability that is not yet fully represented in the current training set.

Text S1. DASNet architecture

DASNet performs joint detection and instance segmentation on two-dimensional DAS data (time \times channel). The model predicts bounding boxes, class labels, and per-instance masks, from which signal arrival times can be estimated for each channel. The architecture consists of several stages described below.

Backbone and feature pyramid network. A ResNet-50 backbone is used to extract hierarchical features from the input DAS image. Feature maps from four backbone stages (with 256, 512, 1024, and 2048 channels, respectively) are fed into a Feature Pyramid Network (FPN), which produces multi-scale feature maps with 128 channels each. These shared features are used by the Region Proposal Network (RPN) as well as the box and mask heads.

Region proposal network. The RPN operates on each FPN level to generate candidate regions of interest. At each spatial location, it predicts objectness scores and bounding-box offsets for multiple anchors with aspect ratios of 0.5, 1.0, and 2.0. Non-maximum suppression (NMS) is applied to remove redundant proposals, and a fixed number of candidate regions are retained and passed to subsequent detection branches.

Box head. Candidate regions are extracted from the feature pyramid using multi-scale RoIAlign with an output resolution of 7×7 . The pooled features are processed by two fully connected layers and then fed into two prediction heads: a classifier that produces class logits (including background) and a box regressor that refines bounding-box coordinates. During inference, bounding boxes are decoded, filtered using a confidence threshold, and processed with class-wise NMS to produce the final detections.

RoI time-extent normalization. Before mask prediction, the temporal extent of each proposal can be normalized to reduce variability in signal duration while preserving arrival-time information. A scaling factor $\alpha = v_{\text{ref}}\Delta t/\Delta x$ (where v_{ref} is a reference propagation velocity, Δt the sampling interval, and Δx the channel spacing) is used to adjust the proposal time span to $\alpha \times N_{\text{channel}}$. This normalization ensures that the mask branch operates on regions with a bounded temporal extent.

Mask head. After normalization, multi-scale RoIAlign extracts a 42×42 feature region for each proposal. The mask head consists of four 3×3 convolutional layers (256 channels, batch normalization, and ReLU activation), followed by a 2×2 transposed convolution for upsampling and a final 1×1 convolution that outputs per-class mask logits. During training, a weighted binary cross-entropy loss is used, with a Gaussian-smoothed weighting map that emphasizes pixels near signal arrivals and regions with higher confidence.

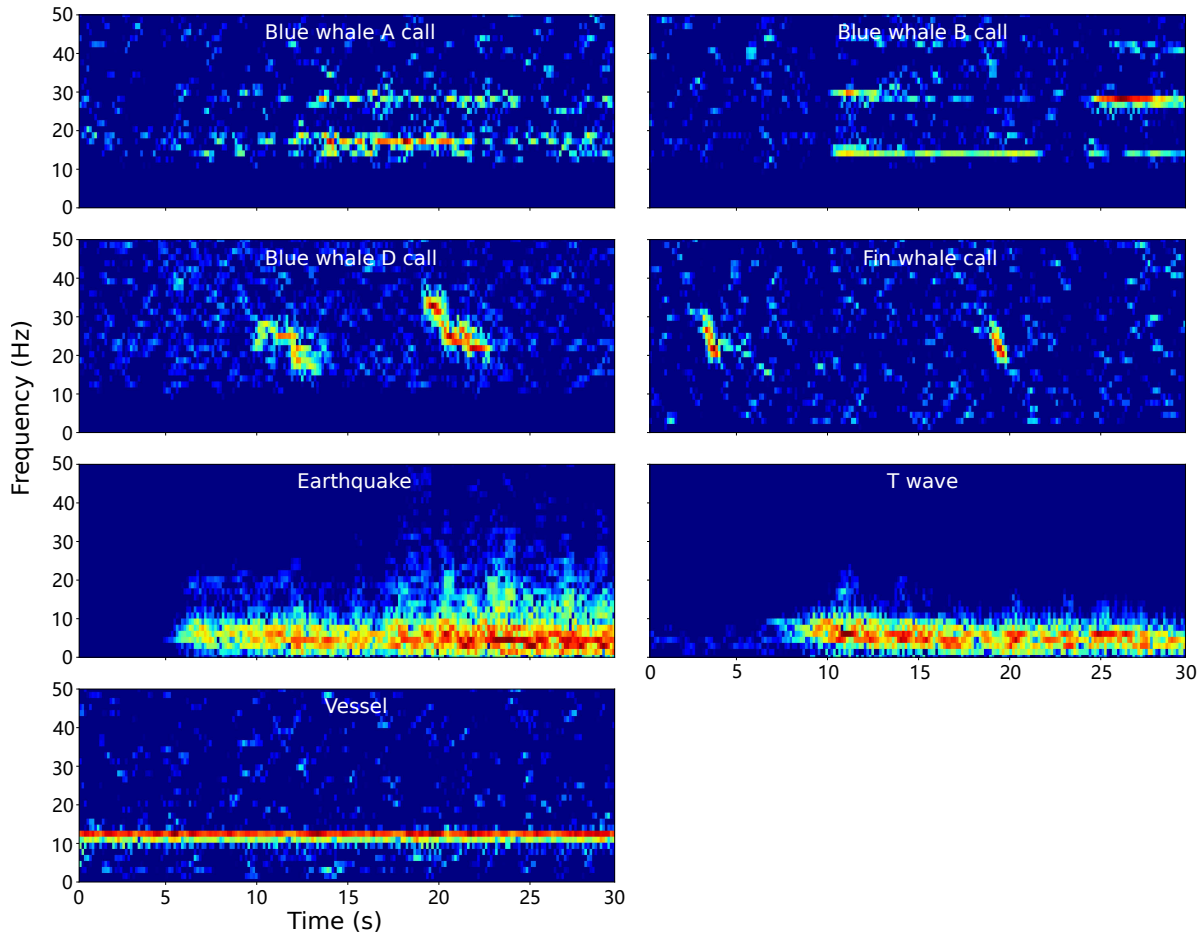


Figure S1: Spectrograms of representative examples for all signal types detected in the SeaFOAM dataset. Each panel shows the spectrogram of a single selected channel from the DAS recording. For whale vocalizations and vessel noise, a 10 Hz high-pass filter was applied, whereas a 2 Hz high-pass filter was used for the other signal types to suppress low-frequency background noise. The displayed spectral amplitudes were limited to a fixed dynamic range to enhance signal visibility.

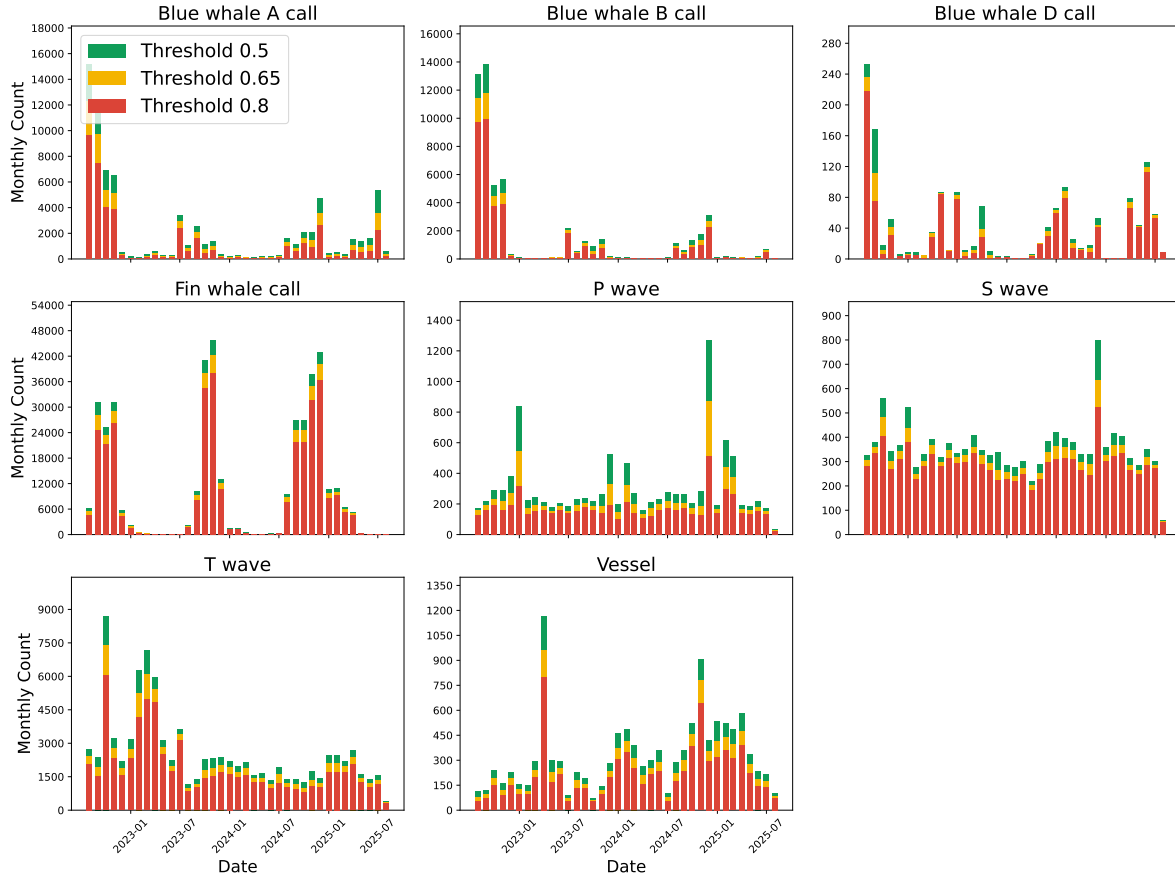


Figure S2: Comparison of DASNet detections across 3 years of continuous data under different score thresholds. Detection counts at lower thresholds co-vary temporally with high-confidence detections, indicating that low-score detections are predominantly associated with real signal activity rather than spurious false positives.

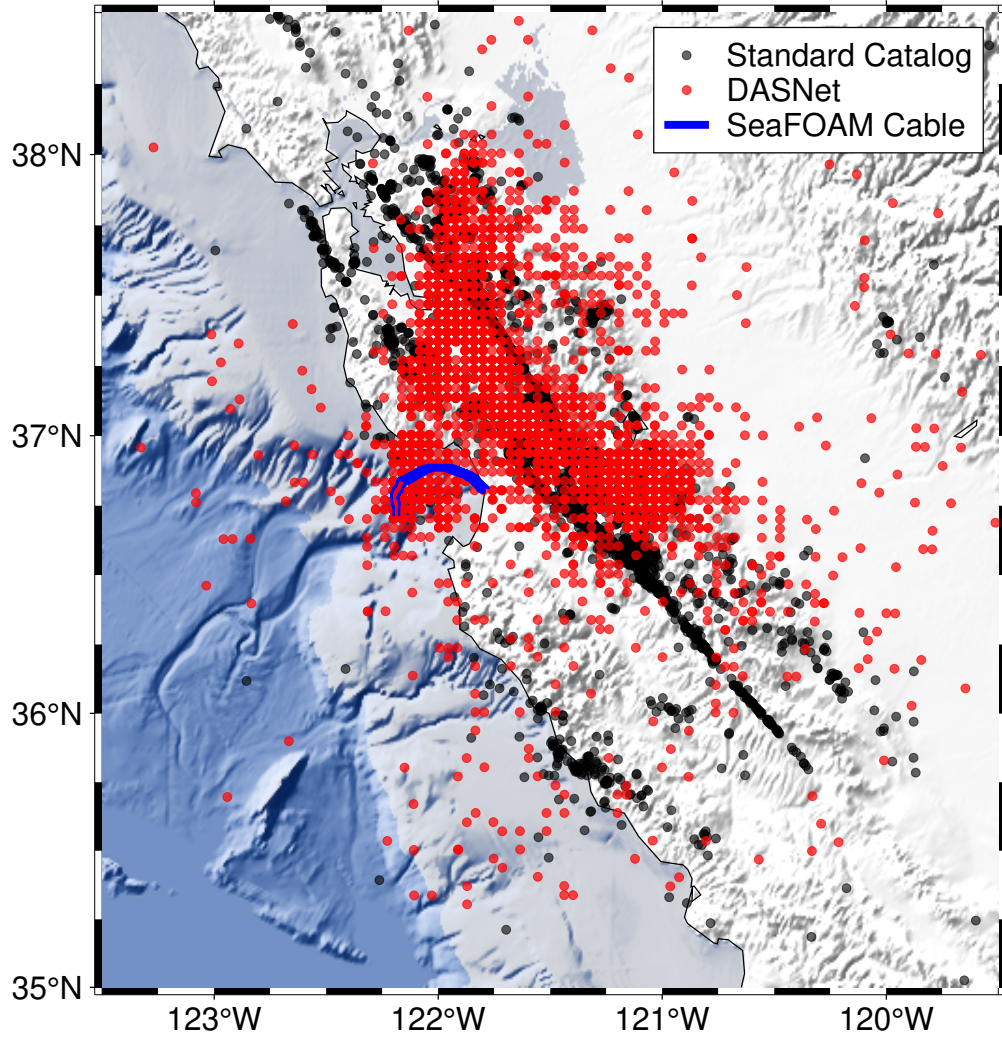


Figure S3: Earthquake locations estimated using P- and S-phase arrival times from the DAS array alone. The DAS-only solutions exhibit increased location uncertainty, especially for events farther from the cable, due to the limited azimuthal coverage of a single linear array. This geometry provides weaker constraints on the back-azimuth and epicentral distance, resulting in larger lateral scatter in the inferred epicenters.

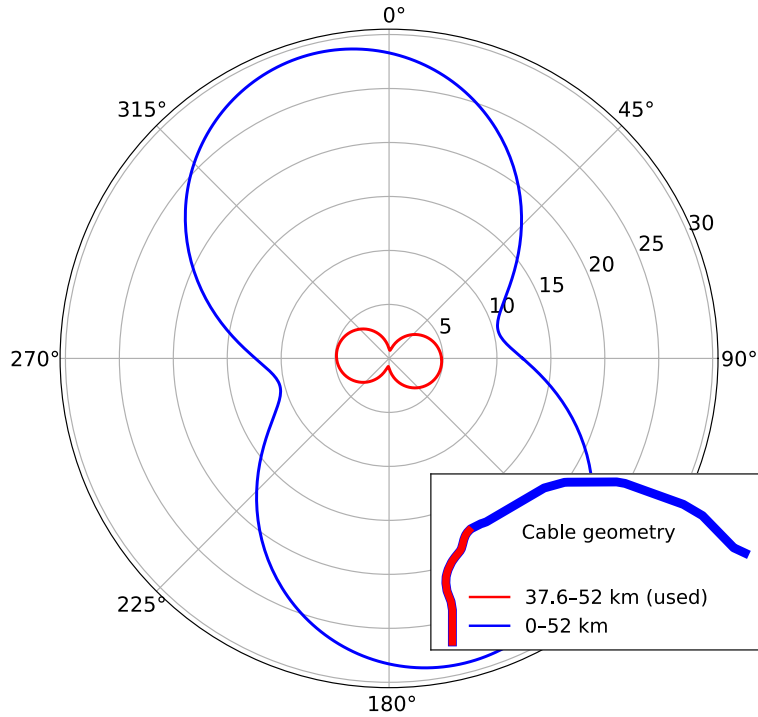


Figure S4: Directional sensitivity of T-wave beamforming. Sensitivity is quantified by measuring how strongly the predicted arrival-time curves across the DAS array change in response to small perturbations in propagation azimuth. The figure compares two cable geometries: the analyzed cable segment and the full cable. Azimuthal constraints are weakest for sources aligned with the cable axis, i.e., along-axis directions yield small inter-channel delay differences. Longer and more curved cable geometries markedly improves azimuthal resolution.

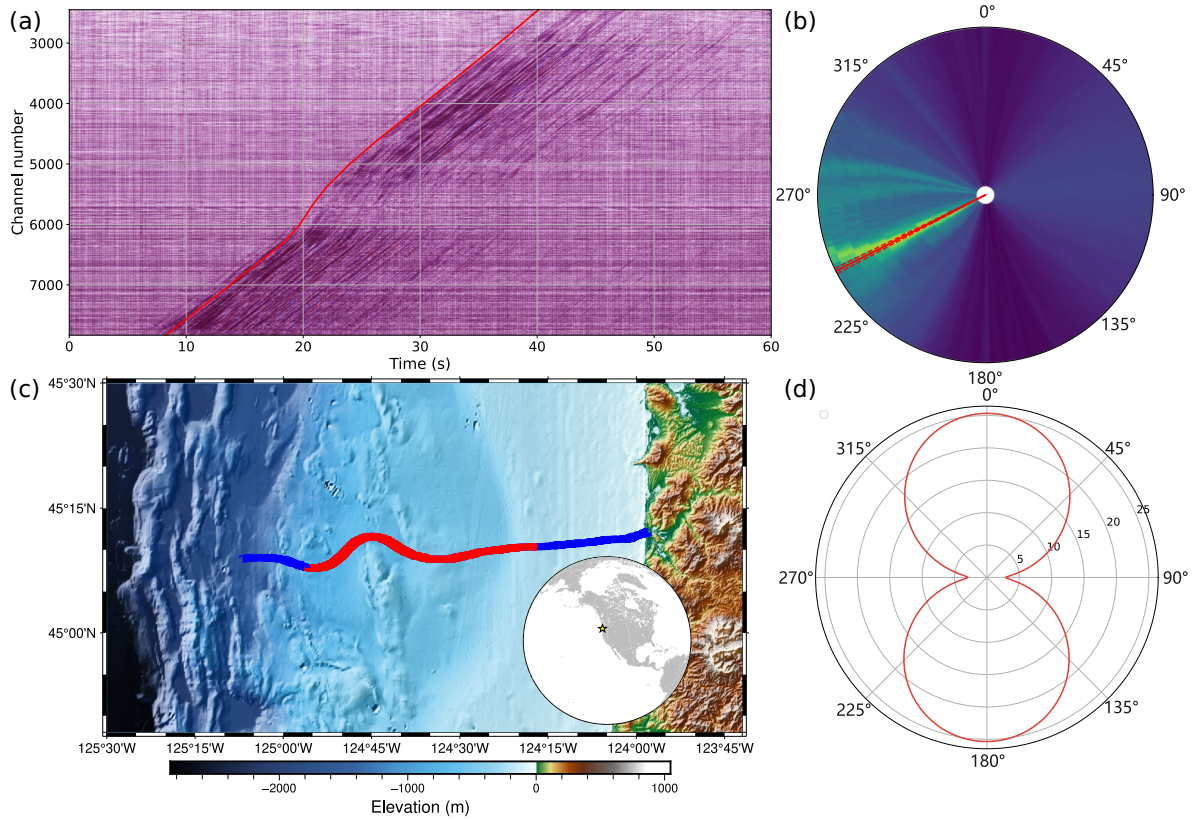


Figure S5: T-wave detection and azimuth estimation using the OOI Regional Cabled Array. (a) T-wave waveforms recorded by the OOI cable, beginning at 2024-05-08 13:38:05 UTC. The red lines show theoretical time difference of arrival computed from the estimated T-wave azimuth in (b). The time offset has been removed. (b) Heatmap derived from beamforming for azimuth estimation. (c) Location and geometry of the OOI cable. (d) Azimuthal sensitivity of the OOI array.

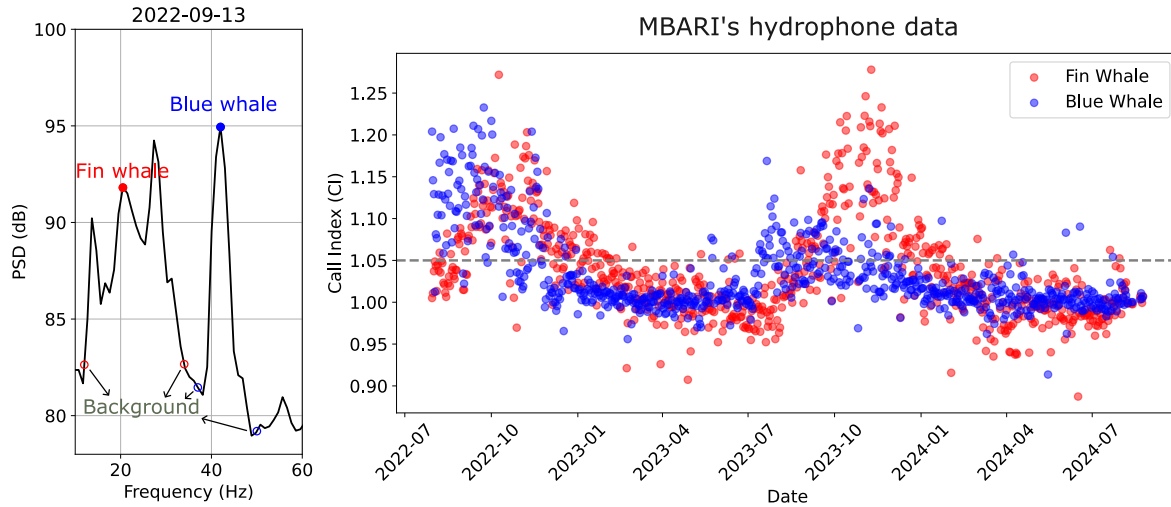


Figure S6: Call Index method for whale acoustic detection from the MBARI hydrophone. (a) Mean spectrum levels measured on 2022-09-13, showing peaks associated with fin whale 20 Hz pulses and the third harmonic of blue whale B calls (around 40 Hz). We compute the Call Index as the ratio of energy at the characteristic frequencies (solid dots) to energy at the background-noise frequencies (open dots). (b) Daily Call Index values. The gray dashed line marks the detection threshold (1.05) used to classify a day as whale-present.

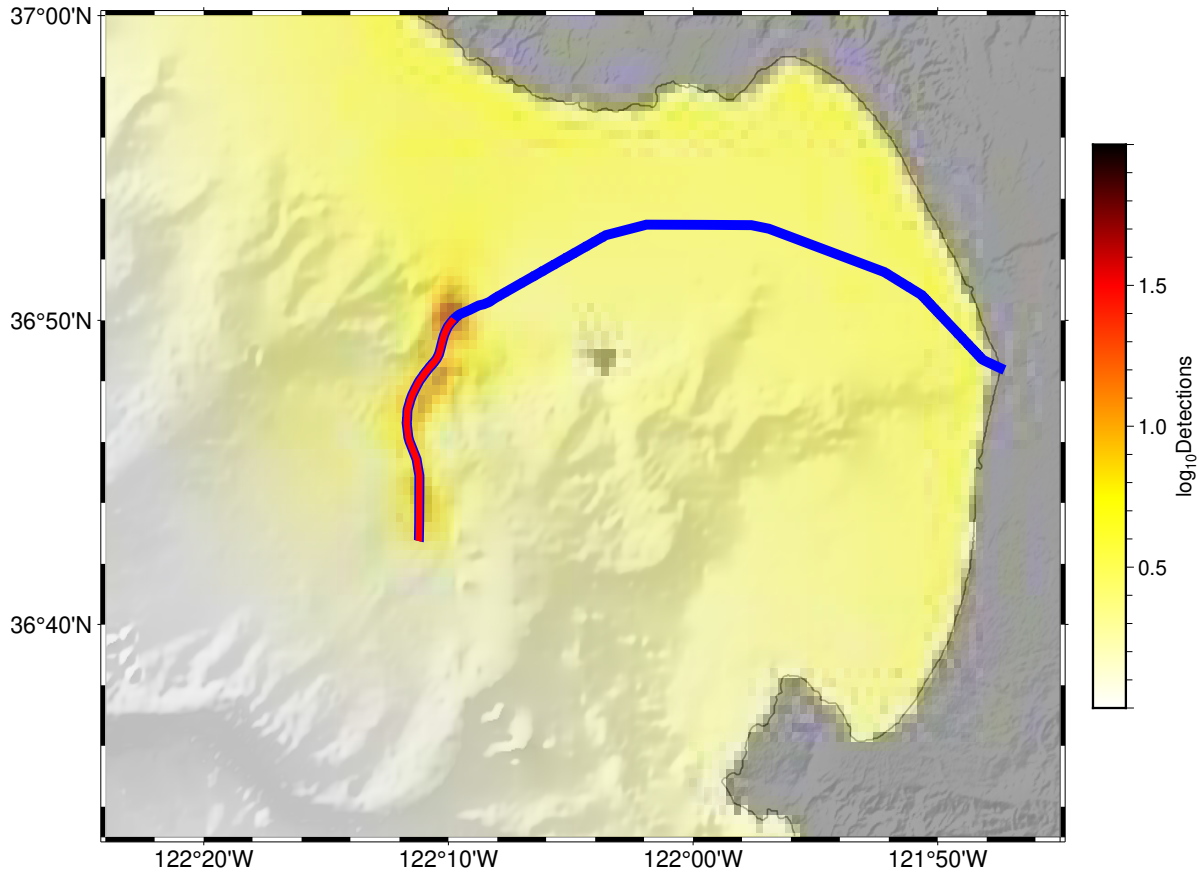


Figure S7: Spatial distribution of blue whale calls over the three-year record. Compared to fin whales (Figure 4b in the main text), blue whales produce fewer calls.

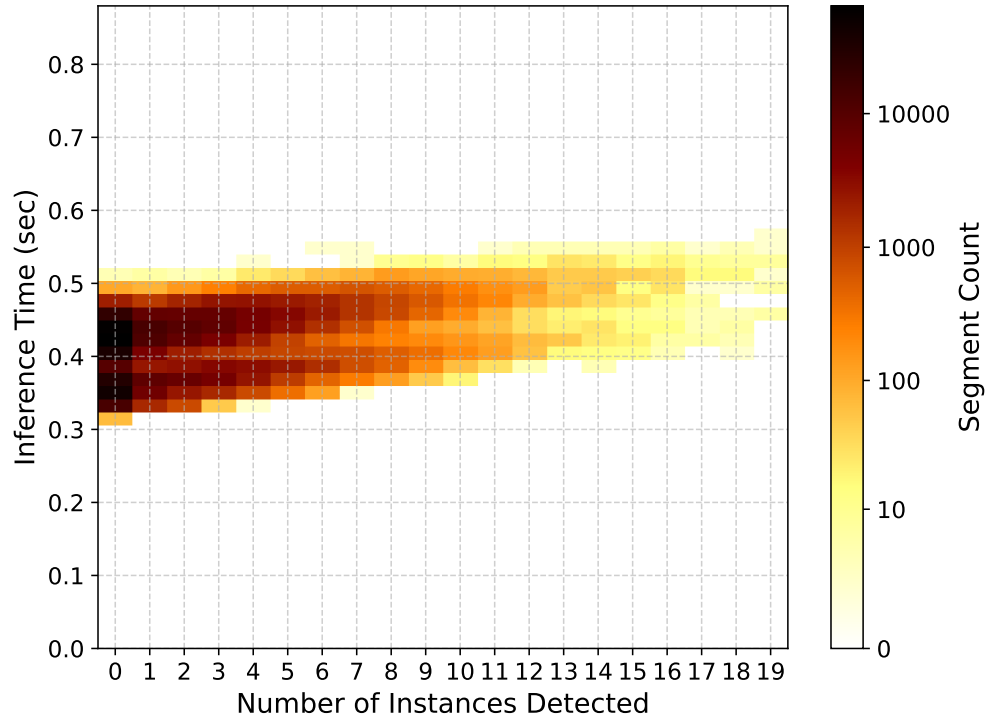


Figure S8: Inference time statistics for DASNet. Each input segment contains 2,845 channels and 12,000 time samples (60 s at 200 Hz). The x-axis shows the number of region proposals per segment that pass the first-stage filtering and are processed by the second-stage detection heads, and the y-axis shows the corresponding inference time. Inference time increases modestly with instance count but remains consistently low, supporting real-time monitoring applications.

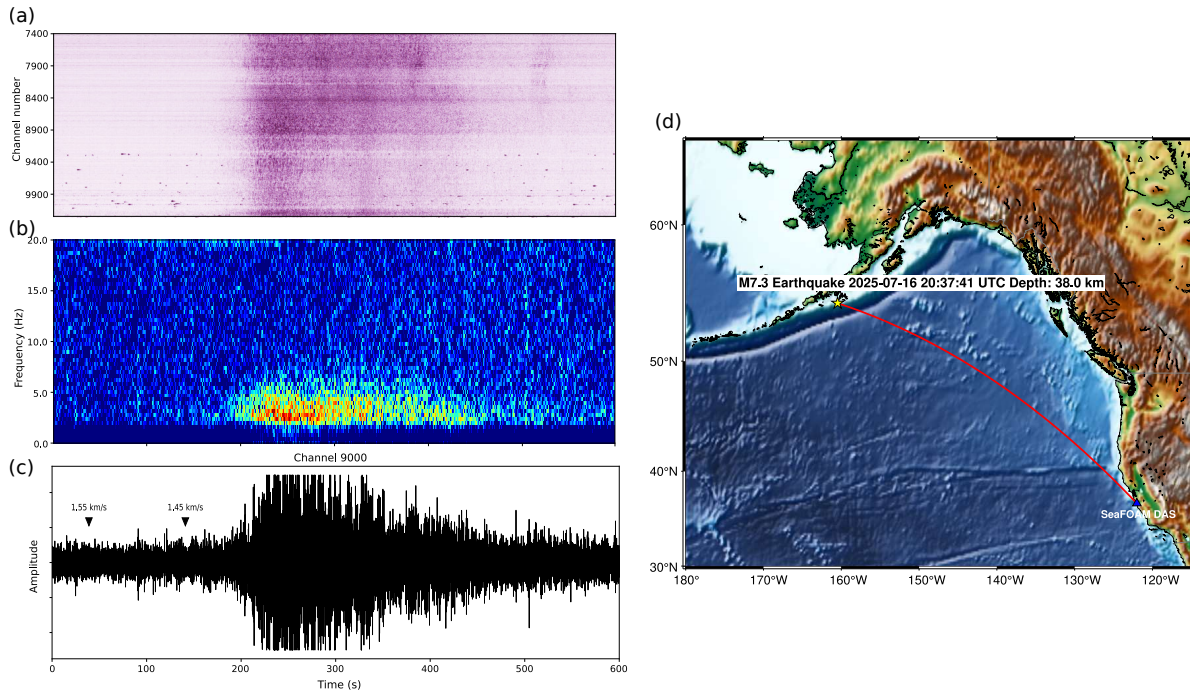


Figure S9: Example of a candidate T-wave from the North Pacific. (a) Spatio-temporal representations for the recorded signal. (b) Spectrogram for Channel 9,000, highlighting enhanced energy primarily in the 2-10 Hz band during the signal interval. (c) 2-10 Hz bandpass-filtered waveform for Channel 9000, with inverted triangles indicating predicted arrival times corresponding to assumed propagation velocities of 1.55 km/s and 1.45 km/s. (d) Map view showing the epicenter of the M7.3 earthquake on 16 July 2025 and the great-circle path (red curve) to the SeaFOAM DAS array.